PNNL-15452 Rev.1

Pacific Northwest National Laboratory
Operated by Battelle for the U.S. Department of Energy

CFEST
Coupled Flow, Energy & Solute Transport
Version CFEST005
Theory Guide

V. L. Freedman
Y. Chen
S. K. Gupta

November 2005

Prepared for the U.S. Department of Energy
under Contract DE-AC05-76RL01830

DISCLAIMER

PACIFIC NORTHWEST NATIONAL LABORATORY
operated by

BATTELLE
for the
UNITED STATES DEPARTMENT OF ENERGY
under Contract DE-AC05-76RL01830

Printed in the United States of America
Available to DOE and DOE contractors from the
Office of Scientific and Technical Information,
P.O. Box 62, Oak Ridge, TN 37831-0062;
ph: (865) 576-8401
fax: (865) 576-5728
email: reports@adonis.osti.gov

Available to the public from the National Technical Information Service,
U.S. Department of Commerce, 5285 Port Royal Rd., Springfield, VA 22161
ph: (800) 553-6847
fax: (703) 605-6900
email: orders@ntis.fedworld.gov
online ordering: http://www.ntis.gov/ordering.htm


This document was printed on recycled paper.
(9/2004)

CFEST
Coupled Flow, Energy & Solute Transport
Version CFEST005
Theory Guide

V. L. Freedman
Y. Chen
S. K. Gupta

November 2005

Prepared for
the U.S. Department of Energy
under Contract DE-AC05-76RL01830

Pacific Northwest National Laboratory
Richland, Washington 99352

Summary

This document presents the mathematical theory implemented in the CFEST (Coupled Flow, Energy, and Solute Transport) simulator. The simulator is a three-dimensional finite element model that is used to evaluate flow and solute mass transport. Although the theory for thermal transport is presented in this guide, it has not yet been fully implemented in the simulator. The flow module is capable of simulating both confined and unconfined aquifer systems, as well as constant and variable density fluid flows. For unconfined aquifers, the model uses a moving boundary for the water table, deforming the numerical mesh so that the uppermost nodes are always at the water table. For solute transport, changes in concentration of a single dissolved chemical constituent are computed for advective and hydrodynamic transport, linear sorption represented by a retardation factor, and radioactive decay. Once fully implemented, transport of thermal energy in the groundwater and solid matrix of the aquifer can also be used to model aquifer thermal regimes.

Mesh construction employs "collapsible" hexahedral finite elements in a three-dimensional coordinate system. CFEST uses the Galerkin finite element method to convert the partial differential equations to algebraic form. To solve the coupled equations for momentum, solute, and heat transport, sequential iteration is used to treat nonlinearities. An upstream weighted residual finite-element method is used to solve the advective-dispersive transport and energy transfer equations. This method circumvents numerical oscillation problems. Matrix solutions of the flow and transport problems are performed using efficient iterative methods in ITPACK, NSPCG and PETSc, solvers available in the public domain. These solvers are based on the preconditioned conjugate gradient and ORTHOMIN methods for symmetric and nonsymmetric matrixes, respectively.

Contents

Figures

Tables

1.0 Introduction

CFEST, which is an acronym for Coupled Flow, Energy and Solute Transport, is a three-dimensional finite-element simulator for analyzing isothermal and nonisothermal groundwater flow, energy, and solute transport problems. For more than two decades, the CFEST simulator has been used to evaluate flow and transport for groundwater basins, Superfund sites, and waste disposal sites. It has also been used at the U.S. Department of Energy (DOE) Hanford Site to predict flow and contaminant transport. This document has been written in support of the ongoing modeling efforts at the Hanford Site.

This document is the first in a series that updates an earlier manual (Gupta et al. 1987) that described model theory, served as a user's guide, and provided user application examples within a single tome. This document is based on the theory provided in the original manuscript and also updates theory related to capabilities developed since that manuscript was published. To this end, this document provides CFEST users with information about the solved governing and constitutive equations, numerical algorithms, and solution techniques. This updated Theory Guide will eventually be accompanied by updated user's and applications guides.

In brief, this document describes the application of the fundamental and empirical models used in the solution of groundwater flow and transport problems formulated in the CFEST simulator. In Chapter 2, a detailed description of the governing conservation equations for water and solute mass is presented. These governing equations for flow and transport are presented as partial differential equations. In Chapter 3, the numerical formulation used to solve the governing equations is described. In the fourth and final chapter, verification problems are presented. For users interested in information on the data input for CFEST, this information will be presented in the updated user's guide. However, until the user's guide is published, the reader is referred to Gupta et al. (1987) and Gupta (1997) for a description of the input data files needed for the numerical simulation.

Although the input structure and governing equations for heat transport have been implemented in CFEST, the solver has not yet been updated for heat transport in the CFEST simulator. Hence, this guide presents the theory associated with thermal transport, even though, as of the time of publication, non-isothermal flow simulations cannot be performed. In subsequent revisions of this theory guide, thermal transport, as well as flow and solute transport, will be updated according to the current state of implementation within the CFEST simulator.

2.0 Governing Equations

The CFEST simulator solves three-dimensional (3-D) groundwater flow, energy, and solute transport problems using the Galerkin finite-element method. The simulator can be used for both confined and unconfined aquifers and either density-dependent or constant density flow simulations. Phreatic (unconfined) solutions can be computed for the uncoupled equations through an iterative technique that adjusts the saturated thickness so that the calculated head is at the top of the system. Solute transport is simulated through numerical solution of a solute mass balance equation where concentration may affect fluid density. The single solute species may be transported conservatively or may undergo equilibrium sorption or decay. Once fully implemented, heat transfer will be simulated through numerical solution of an energy balance equation, where fluid density and viscosity may be affected by temperature.

Governing equations for momentum, heat, and mass transport are the fundamental equations solved in the simulator [see, for example, Bear (1979), Freeze and Cherry (1979), or Domenico and Schwartz (1990)]. Applications of CFEST, therefore, are limited by the assumptions inherent in the constitutive theory and the methods for solving the governing partial differential equations.

Associated with constitutive theory for flow, it is assumed that fluid flow is laminar. Assuming a compressible fluid and porous medium, transient flow is described using Darcy's law for advection. CFEST also solves transient transport of contaminants with decay, adsorption, and velocity-dependent dispersion. Because only a single aqueous phase is considered, all fluids are regarded as completely miscible. For heat transfer, kinetic and potential energy components are neglected.

All boundary conditions, sources, and sinks can be spatially and time variant. Boundary conditions may be prescribed nodal head or prescribed flow as a function of time or head-dependent flow. For solute transport, boundary conditions may be either prescribed nodal concentration or prescribed mass flux. Temperature or gradient boundary conditions may be specified for the heat transfer equation. Prescribed energy fluxes may also be specified for simulating heat transfer.

Hydrogeologic properties can be spatially varied throughout the computational domain within the resolution of the finite element discretization. Material properties such as porosity and permeability are associated with grid elements. Because irregularly shaped elements can be used, a material thickness is defined by the nodes as the distance between upper and lower nodes within the grid element. An assumption of permeability and coordinate axes colinearity is also associated with the use of the finite element grid. That is, variations between anisotropic axes and coordinate axes are assumed to be insignificant.

In the paragraphs that follow, the mathematical formulations of the governing equations and constitutive relationships are presented. This is followed by a description of the finite-element formulations implemented in the CFEST simulator.

2.1 Water Mass Conservation Equation

The CFEST simulator represents fluid flow through saturated porous media. For variable density flow, this involves the solution of pressure (P) [N m^{-2}] as one of the primary variables. The mass conservation or continuity equation used to describe transient, density-dependent groundwater flow in a porous medium is given as

$$-\nabla \cdot \rho q + \Omega = \frac{\partial(\theta\rho)}{\partial t} \tag{2.1}$$

where θ is the porosity [$m^3 m^{-3}$], ρ is the fluid density [kg m^{-3}], *t* is time [s], and ∇ is the divergence operator. The Darcy flux q [m s^{-1}] is an empirical relationship that describes the discharge rate through a porous medium to the pressure gradient and is given as

$$q = \frac{-k}{\mu}(\nabla P + \rho g \nabla z) \tag{2.2}$$

where k is the intrinsic permeability [m^2], μ is the fluid dynamic viscosity [N s m^{-2}], g is the gravitational acceleration [m s^{-2}], and z is the depth of a reference point to a standard datum [m]. In CFEST, fluid viscosity is a function of temperature and concentration.

Pressure differentials between source and sink terms may be significant in deep aquifers (INTERCOMP 1976). Hence, the source/sink volume flux per unit volume in Eq. (2.1), Ω [kg $m^{-3} s^{-1}$], is expanded to yield

$$\Omega = \left(\Omega_{in} + P_{in}\frac{d\Omega_{in}}{dP}\right) + \left(\Omega_{out} + P_{out}\frac{d\Omega_{out}}{dP}\right) \tag{2.3}$$

where Ω_{in} represents a mass source (positive for in flow) and Ω_{out} represents a mass sink (negative for out flow). For clarity in the discussion that follows, the symbol Ω is used to represent both the sink and source terms given in Eq. (2.3).

-

The CFEST simulator is also capable of simulating steady-state flow solutions. In this case, the time-dependence term is removed from the right side of Eq. (2.1) and is replaced with a zero to represent no changes in storage for the mass of fluid in the system.

2.1.1 Constant Density

For applications where density is either constant or only a function of pressure, the continuity equation given in Eq. (2.1) can be solved in terms of hydraulic head rather than pressure. The relationship between hydraulic head and pressure is defined as

$$h = \frac{P}{\rho g} + z \tag{2.4}$$

where h represents the hydraulic head [m]. Substituting Eq. (2.4) into Eq. (2.2) yields

$$q = -\mathrm{K} \bullet \nabla h \tag{2.5}$$

where K is the hydraulic conductivity tensor [m s^{-1}] and is expressed as

$$K = \frac{k\rho g}{\mu} \tag{2.6}$$

Hydraulic conductivity is known as the proportionality constant in Darcy's law, which relates the amount of water that flows through a unit cross-sectional area under a unit gradient of hydraulic head.

Using the chain rule for differentiation, the right side of Eq. (2.1) can be written as

$$\frac{\partial(\theta\rho)}{\partial t} = \theta\frac{\partial\rho}{\partial t} + \rho\frac{\partial\theta}{\partial t} \tag{2.7}$$

where the first term on the right side of Eq. (2.7) is related to the expansion of the fluid (β ,[N^{-1}]), and the second term describes the compressibility of the porous medium (α ,[N^{-1}]). The specific storage of an aquifer, S_s [m^{-1}], describes the volume of water released from storage due to expansion of water and matrix compression per unit decline in head and is given as

$$S_s = \rho g(\alpha + \theta\beta) \tag{2.8}$$

Assuming constant density $\left(\partial\rho/\partial t = 0\right)$ and incorporating the concept of specific storage into Eq. (2.7), Eq. (2.7) becomes

$$\frac{\partial(\theta\rho)}{\partial t} = \rho S_s\frac{\partial h}{\partial t} \tag{2.9}$$

As a final step, substituting Eq. (2.9) into the right side of Eq. (2.1), the following equation can be used to solve for transient head in confined aquifers under an assumption of constant density:

$$\nabla\mathrm{K} \bullet \left(\nabla h\right) + \Omega = S_s\frac{\partial h}{\partial t} \tag{2.10}$$

For unconfined aquifers, the water volumes associated with water expansion and pore space contraction are small compared with the water volumes obtained from pore drainage. The specific yield (S_y) [m^{-1}] is the storage term in unconfined aquifers and is defined as the water volume obtained from pore drainage. Because the specific yield is assumed to be equivalent to porosity in the CFEST simulator, Eq. (2.10) for unconfined aquifers becomes

$$\nabla \mathrm{K} \bullet (\nabla h) + \Omega = \theta \frac{\partial h}{\partial t} \tag{2.11}$$

For confined aquifers, matrix porosity is defined as a function of pressure, given as

$$\theta \approx \theta_0 [1 + \alpha (P - P_o)] \tag{2.12}$$

where θ_o the initial porosity of the medium. The constitutive relationship between matrix porosity and hydraulic head for confined aquifers in terms of pressure and in terms of head is defined with Eq. (2.13):

$$\frac{\partial \theta}{\partial t} = (\theta_o \alpha) \frac{\partial P}{\partial t} = (\rho g \theta_o \alpha) \frac{\partial h}{\partial t} \tag{2.13}$$

2.1.2 Variable Density Formulation

For variable density formulations, the specific storage term cannot be used because it assumes a fluid of constant density. To model variable density systems, fluid density is considered to be a function of solute concentration (C), temperature (T), and pressure (P). Using a Taylor series expansion, the density function can be expressed as

$$\begin{aligned} \rho(C,T,P) = \rho_o(E_o) + \left[\frac{\partial \rho}{\partial C}(C - C_o) + \cdots \right] + \\ \left[\frac{\partial \rho}{\partial T}(T - T_0) + \cdots \right] + \left[\frac{\partial \rho}{\partial P}(P - P_0) + \cdots \right] \end{aligned} \tag{2.14}$$

where ρ_o is the initial aquifer density as a function of the concentration, temperature , and pressure conditions ($E_o = (C_o, T_o, P_o)$). Neglecting higher-order terms in the Taylor series, the chain rule expansion shown in Eq. (2.7) and the porosity derivative shown in Eq. (2.14) can be rewritten as

$$\begin{aligned} \frac{\partial(\theta\rho)}{\partial t} &= \theta \frac{\partial \rho}{\partial t} + \rho \frac{\partial \theta}{\partial t} \\ &= \theta \rho_o \left(C_w \frac{\partial P}{\partial t} + C_T \frac{\partial T}{\partial t} + C_c \frac{\partial C}{\partial t} \right) + \rho(\theta_o \alpha) \frac{\partial P}{\partial t} \end{aligned} \tag{2.15}$$

where C_w is the fluid compressibility [$m^2 N^{-1}$], C_T is the coefficient of thermal expansion [$°C^{-1}$], and C_c is a composition density ratio [kg mol^{-1}] that is assumed to be constant and defined as

$$C_w = \frac{1}{\rho_o} \frac{\partial \rho}{\partial P} \tag{2.16}$$

$$C_T = \frac{1}{\rho_o} \frac{\partial \rho}{\partial T} \tag{2.17}$$

$$C_c = \frac{1}{\rho_o}\frac{\partial \rho}{\partial C} \tag{2.18}$$

For clarity, let Γ represent the variables in the first term on the right side of Eq. (2.15):

$$\Gamma = \left(C_w \partial P + C_T \partial T + C_c \partial C\right) \tag{2.19}$$

so that Eq. (2.15) can be expressed in shorthand notation as

$$\frac{\partial(\theta\rho)}{\partial t} = \rho_o \theta \frac{\partial \Gamma}{\partial t} + \rho(\theta_o \alpha)\frac{\partial P}{\partial t} \tag{2.20}$$

2.1.3 Density Dependence on Temperature

As discussed in Section 2.1.2, fluid density may be considered a function of temperature. For simulating the density dependence on temperature, the following empirical relationships from Tsang et al. (1980) can be applied:

$$\begin{aligned} \rho(T) &= a\left[1 - b_1(T-25) - b_2(T-25)^2\right] \qquad 25\ ^\circ C \le T \le 100^\circ C \\ \rho(T) &= a\left[1 - b_3(T-25)\right] \qquad\qquad T < 25\ ^\circ C \end{aligned} \tag{2.21}$$

where T represents the temperature (°C) and a, b_1, b_2, and b_3 are constants with values of 996.9, 3.17×10^{-4}, 2.56×10^{-6}, and 1.87×10^{-4}, respectively.

2.2 Solute Mass Conservation Equation

The solute conservation equation equates the time rate of change of solute within a volume with the solute flux crossing the volume surface. Hence, transient advective-dispersive transport in saturated porous media is described as

$$\nabla \cdot \left(\theta\rho D \nabla C\right) - \nabla\left(\rho q C\right) - \theta\rho R_f \lambda C + \Omega_c = \frac{\partial\left(\theta\rho C\right)}{\partial t} R_f \tag{2.22}$$

where C is the solute concentration [mol kg^{-1}], D is the coefficient of hydrodynamic dispersion [$m^2\ s^{-1}$], and Ω_c is a general source or sink term representing an addition or a loss of mass [mol $m^{-3}s^{-1}$]. The types of reactions incorporated into CFEST are restricted to those that can be represented by a first-order rate reaction such as radioactive decay. The first-order radioactive decay constant for both the free and sorbed solute, λ [s^{-1}], is defined as

$$\lambda = \frac{\ln(2)}{t_{1/2}} \tag{2.23}$$

where $t_{1/2}$ is the solute half-life, the time for the chemical to decay to half its original concentration. A retardation factor that represents instantaneous, reversible, sorption-desorption reactions governed by a linear isotherm and constant distribution coefficient, (K_d) [mLg^{-1}], is given by the dimensionless retardation factor, R_f:

$$R_f = 1 + \frac{K_d \rho_b}{\theta} \tag{2.24}$$

where ρ_b is the bulk density of the porous media [kg m^{-3}]. Changes in the retardation factor due to transient flow effects on porosity are assumed to be insignificant, and the retardation factor is assumed to be time invariant.

Assuming that concentration (C), temperature (T), and pressure (P) are coupled, the time derivative in Eq. (2.22) can be written as

$$\frac{\partial(\theta\rho C)}{\partial t} = (\rho C)\alpha\theta_o \frac{\partial P}{\partial t} + (\rho_0 \theta C)\frac{\partial \Gamma}{\partial t} + (\rho\theta)\frac{\partial C}{\partial t} \tag{2.25}$$

Note that Eq. (2.25) incorporates the shorthand notation for the Taylor series expansion for density as a function of the three primary variables shown in Eq. (2.16).

2.2.1 Sinks and Sources

Similar to the definition of the sink/source term in Eq. (2.1) describing the conservation of momentum, flux differentials with respect to pressure may exist for the sink/source term in Eq. (2.22). Accounting for both inflow (positive), q_{in}, and outflow (negative), q_{out}, Darcy fluxes, the source/sink term in Eq. (2.22) is written as

$$\Omega_c = \left(q_{in} + P_{di} \frac{dq_{in}}{dP} \right) C_{in} + \left(q_{out} + P_{do} \frac{dq_{out}}{dP} \right) C_{out} + S_r \tag{2.26}$$

where C_{in} and C_{out} are the concentrations in mass per unit mass units for the solute in entering the aquifer and exiting the aquifer, respectively. The input pressure differential (P_{di}) is defined as ($P_{in} - P$), and for outflow, the pressure differential (P_{do}) is defined as ($P_{out} - P$). The term S_r (see Section 2.3.3) represents the solute loading due to salt dissolution. Head differentials are defined in a similar manner for cases of constant density. For clarity in the discussion that follows, only the symbol Ω_c is used to represent both the sink and source terms as given in Eq. (2.26).

2.2.2 Diffusion and Dispersion

The coefficient θD in Eq. (2.22) is the sum of the diffusion and dispersion components given by

$$\theta D_{ij} = (\alpha_L - \alpha_T)\frac{q_i q_j}{|q|} + \alpha_T |q| \delta_{ij} + \theta\tau D_d \delta_{ij} \tag{2.27a}$$

$$\delta_{i,j} = \begin{cases} 1 & i = j \\ 0 & i \neq j \end{cases} \tag{2.27b}$$

where α_L [m] and α_T [m] are the longitudinal and transverse dispersivities, respectively; τ is the matrix tortuosity [m]; and D_d is the free solution diffusion coefficient [m^2s^{-1}]. The Kronecker delta, δij, is equal to one if $i = j$ and zero if $i \neq j$, as shown in Eq. (2.27b). This formulation for dispersion is based on Scheidegger's (1961) finding that a homogeneous isotropic medium can have no more than two independent dispersivity factors. When the velocity vector is divided into components along the three coordinate axes, nine components of the dispersivity tensor result.

For unconfined aquifers, the effective porosity (θ) in Eq. (2.22) and 2.27) is assumed to be equivalent to the specific yield in Eq. (2.9). Although assuming that effective porosity is equivalent to total porosity may be reasonable for some aquifer materials, for other material types such as clays some of the pore space may be too small or too poorly connected to permit the water they contain to drain very easily. In these cases, the effective porosity is less than the total porosity, and the resulting pore velocity (q/θ) is underestimated.

2.2.3 Salt Dissolution Submodel

Because salt beds and domes are likely candidates for nuclear waste storage sites and are also pertinent to the occurrence of petroleum, a salt dissolution submodel is incorporated into the CFEST simulator. The salt source (S_r) (kg m^{-3}) is treated explicitly in Eq. (2.22) and is associated with the sink/source term (Ω_c) in the transport equation given in (2.26). The salt submodel is based on a dissolution model by Ross et al. (1982) and represents the rate at which salt mass is introduced to the fluid per unit volume of aquifer:

$$S_r = \theta \rho \, k_t \chi \frac{(C_s - C)}{(1 + C)} \tag{2.28}$$

where C_s is the saturated brine concentration [kg(salt) $kg(H_2O)^{-1}$], k_t [s^{-1}] is the first-order rate constant for the pure salt, and χ is the mass fraction of the soluble mass to the total solid mass of the aquifer formation.

2.3 Heat Conservation Equation

In CFEST, energy is transported by flow of groundwater and thermal conduction from higher to lower temperatures through both the fluid and the solid matrix. The energy conservation equation in Eq. (2.29) states that the time-rate change of energy within a defined volume is equal to the total flux of energy crossing that volume surface. Assuming a constant effective thermal conductivity for both the fluid and matrix, transient diffusive-dispersive and convective thermal transport can be described as

$$\nabla \theta \kappa \bullet (\nabla T) - \nabla T \bullet (\theta \rho q c_p) + \Omega_T = \frac{\partial (T \rho' c')}{\partial t} \tag{2.29}$$

where T is the temperature [°C], c_p is the specific heat of the fluid [J kg^{-1} °C^{-1}], Ω_T [Wm^{-2}] is a heat sink/source term, and $\rho' c'$ is an effective heat capacity for the unit volume.

2.3.1 Dispersive Transport

The thermal conductivity tensor in Eq. (2.29), κ [W m^{-1} °C^{-1}], is a term that accounts for dispersion and diffusion of heat by convective flow and the heat conductivity of the aquifer and is defined as

$$\theta\kappa = \theta\left(\kappa_e + D_e \rho c_p\right) \tag{2.30}$$

where κ_e represents the thermal diffusion coefficient [W m^{-1} °C^{-1}], and D_e [m] represents the thermal dispersivity. In CFEST, it is assumed that hydrodynamic dispersion predominates over thermal diffusion, and the thermal diffusion coefficient (κ_e) is assumed to be negligible. Thus, the energy dispersion term is determined in a manner similar to the hydrodynamic dispersion given in Eq. (2.27a):

$$\begin{aligned}\left(\theta\rho c_p\right)D_{e_{ij}} = (\alpha_L - \alpha_T)\frac{q_i q_j}{|q|}\left(c_p\rho\right) + \\ \alpha_T |q|\left(c_p\rho\right)\delta_{ij} + \theta\tau\left(\rho c_p\right)D_m\delta_{ij}\end{aligned} \tag{2.31}$$

where D_m is the molecular heat conductivity for both the fluid and porous media [W m^{-1} °C^{-1}]. Eq. (2.31) accounts for contributions to locally stored energy from hydrodynamic diffusion and dispersion.

2.3.2 Sinks and Sources

Accounting for both inflow (positive), q_{in}, and outflow (negative), q_{out}, Darcy fluxes, the thermal source/sink term, Ω_T, is a heterogeneous term that can be expressed as

$$\Omega_T = \left(c_p T\right)_{in}\left(q_{in} + P_{di}\frac{dq_{in}}{dP}\right) + \left(c_p T\right)_{out}\left(q_{out} + P_{do}\frac{dq_{out}}{dP}\right) + \dot{Q} \tag{2.32}$$

where $(c_pT)_{in}$ and $(c_pT)_{out}$ represent the input and output quantity of heat, respectively, and $\dot{Q}$ represents an energy sink/source from confining layers [W m^{-3}]. This source term is based on a vertical temperature gradient in the confining media that yields a one-dimensional (1-D) energy conduction expression given as

$$\dot{Q} = \frac{\partial T}{\partial z}c_p\rho \tag{2.33}$$

For clarity in the following discussion, the symbol Ω_T is used to represent all sink/source terms presented in Eq. (2.32).

2.3.3 Time Derivative

The time derivative in Eq. (2.29) expresses the total change in energy stored in both the solid matrix and fluid per total unit volume. For the fluid component of the volume, the quantity of heat gained or lost is represented by $\theta\rho c_p$. For the porous matrix, this quantity can be expressed as $(1-\theta)\rho_b c_s$. Hence, the effective heat capacity for the entire volume is defined as

$$\rho' c' = \theta\rho c_p + (1-\theta)\rho_b c_s \tag{2.34}$$

where c_s is the specific heat of the solids [J kg^{-1} °C^{-1}], and ρ_b is the solid bulk density [kg m^{-3}]. Assuming that concentration (C), temperature (T), and pressure (P) are coupled, the time derivative in Eq. (2.29) for the fluid (the first term on the right side of Eq. 2.34) can be written as

$$\frac{c_p \partial(\theta\rho T)}{\partial t} = (c_p \rho T)\alpha\theta_o \frac{\partial P}{\partial t} + (c_p \theta T)\frac{\partial \Gamma}{\partial t} + (c_p \rho\theta)\frac{\partial T}{\partial t} \tag{2.35}$$

where Γ denotes the shorthand notation for the Taylor series expansion for density as a function of the three primary variables (see Eq. 2.18). The time derivative for the solid phase heat transfer from the second-term on the right side of Eq. (2.34) is similarly expressed as

$$\frac{(c_s \rho_b)\partial T}{\partial t} - \frac{(c_s \rho_b)\partial(\theta T)}{\partial t} = c_s \rho_b \frac{\partial T}{\partial t} - \left[(c_s \rho_b \theta)\frac{\partial T}{\partial t} + (c_s \rho_b T)(\alpha\theta_o)\frac{\partial P}{\partial t} \right] \tag{2.36}$$

2.4 Review of Assumptions

Several assumptions for the governing equations and constitutive relationships have been outlined in the previous sections. The following is a list of assumptions that should be evaluated before using CFEST to simulate flow and transport:

1. The porous media and fluid are compressible and in thermal equilibrium.
2. Permeability and coordinate axes are collinear.
3. Specific yield for unconfined aquifers is equivalent to the porosity.
4. Hydrodynamic dispersion is a function of fluid velocity.
5. Only one solute can be simulated and is miscible with the ambient groundwater.
6. No chemical reactions occur that affect aquifer properties.
7. Retardation factors are constant with time.
8. Rock density and heat capacity are time-invariant.

The degree to which field conditions deviate from these assumptions will affect the applicability and reliability of CFEST model predictions. If the deviation from a particular assumption is significant, the governing equations and numerical code may need to be modified to account for appropriate processes.

3.0 Numerical Formulation

Numerical methods are used to solve the coupled equations for flow and transport in CFEST. To this end, the continuous variables of the governing differential equations presented in the previous section are replaced with discrete variables that are defined at grid blocks (elements) or at nodes. Thus, the continuous differential equations that define hydraulic head, solute concentration, or temperature everywhere in the system are replaced with a finite number of algebraic equations that define the head, concentration, and/or temperature at specific points. The resulting system of algebraic equations is solved using the matrix techniques outlined in this section.

Numerical methods do not yield exact solutions, only approximate solutions to the governing equations. Numerical methods require that the governing differential equations be discretized in space and time. The variable internal properties, boundaries, and stresses of the system are approximated within the discretized format. In general, the finer the discretization, the closer the numerical solution is to the true solution.

In this section, the finite element spatial discretization used in CFEST is presented. There is no discussion of the methods for generating an input finite element grid; however, automatic mesh generators and interfaces with geographic information system (GIS) tools have been successful in creating quadrilateral grids for the CFEST simulator. The application of the Galerkin finite element method to the governing equations in CFEST is also discussed in this section. Finally, the matrix equations resulting from the finite element discretization are presented, followed by a description of the solvers.

3.1 Coordinate System and Grid Configuration

CFEST is a 3-D finite element model that uses a Cartesian coordinate system in the x, y, and z directions. CFEST generates a 3-D grid from surface topology and vertical information on the subsurface layers. Model regions are then divided into rectangular and/or orthogonal curvilinear elements. The elements are 3-D, arbitrary hexahedral eight-node bricks (Figure 3.1a), although pseudo-tetrahedral elements may be generated from two-dimensional (2-D) surface elements whose lines share the same vertices (Figure 3.1b). Hexahedral elements are simple to deal with, and their matrixes can be easily computed using efficient numerical methods in CFEST. In addition, regions with irregular boundary geometries can be accurately represented.

3.1.1 Hexahedral Finite Element Grid

Although CFEST can be applied as a 1-D-, 2-D, or 3-D model, the region of space in which flow and transport are to be simulated is always defined in three spatial dimensions. For example, in a 1-D simulation, the bounded volume of the aquifer is divided into a set of contiguous blocks (finite elements) that are organized in layers (see Figure 3.2a). Each element has a 3-D shape, but each block has a unit width and depth. For a 1-D slice through an aquifer, the finite element mesh would be a single “stack” of finite elements. Similarly, for a 2-D simulation, the elements are hexahedral, but the third spatial dimension is a unit depth (Figure 3.2b). For a 3-D grid, a set of contiguous blocks exists in all three coordinate directions (Figure 3.2c).

a)

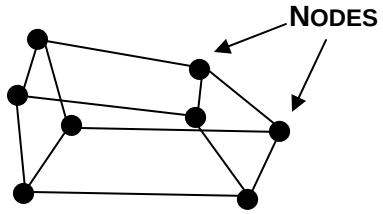

b)

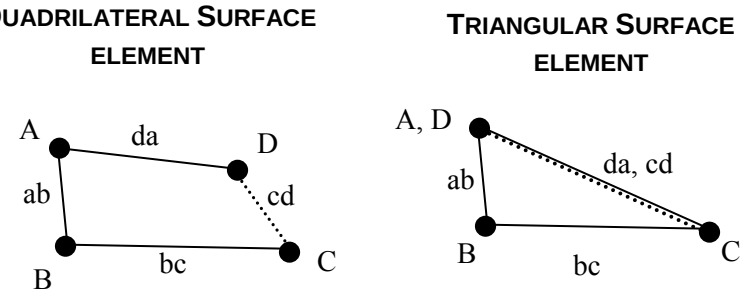

Figure 3.1. Examples of a) an Arbitrary Hexahedral Element Used in the Model Domain for the CFEST Simulator and b) Quadrilateral and Triangular Surface Elements Containing Four Vertices and Four Lines (lines da and cd are the same, and vertex A is equal to vertex D for the triangular element)

3.1.2 Adaptive Gridding for Unconfined Aquifers

For unconfined aquifers, both the hydraulic head distribution and the water table configuration are unknown. The main criterion for accurately simulating the position of the water table is that the elevation of nodes along the water table must be equal to the hydraulic head. Hence, when changes occur in the position of the water table, elements are deformed throughout time, so the node elevation is equal to the hydraulic head. Usually this involves only the top row of elements, but it can include several rows in the domain.

If there is an increase in the water table, the elements in the model domain are stretched vertically. Conversely, if the water table drops, the elements are compressed vertically into a pinched layer. If the mesh contracts through layer boundaries, the initial hydrostratigraphy is still preserved by collapsing the hexagonal elements, so the vertical distance between the two z planes is reduced by a minimal user-defined thickness (e.g., 0.01–0.001 m). The collapsed layers temporarily adopt the same material properties of the current saturated layer. Because the elements are not eliminated from the domain, if the water table rises again, the collapsed elements are expanded so the hydraulic head matches the water table elevation.

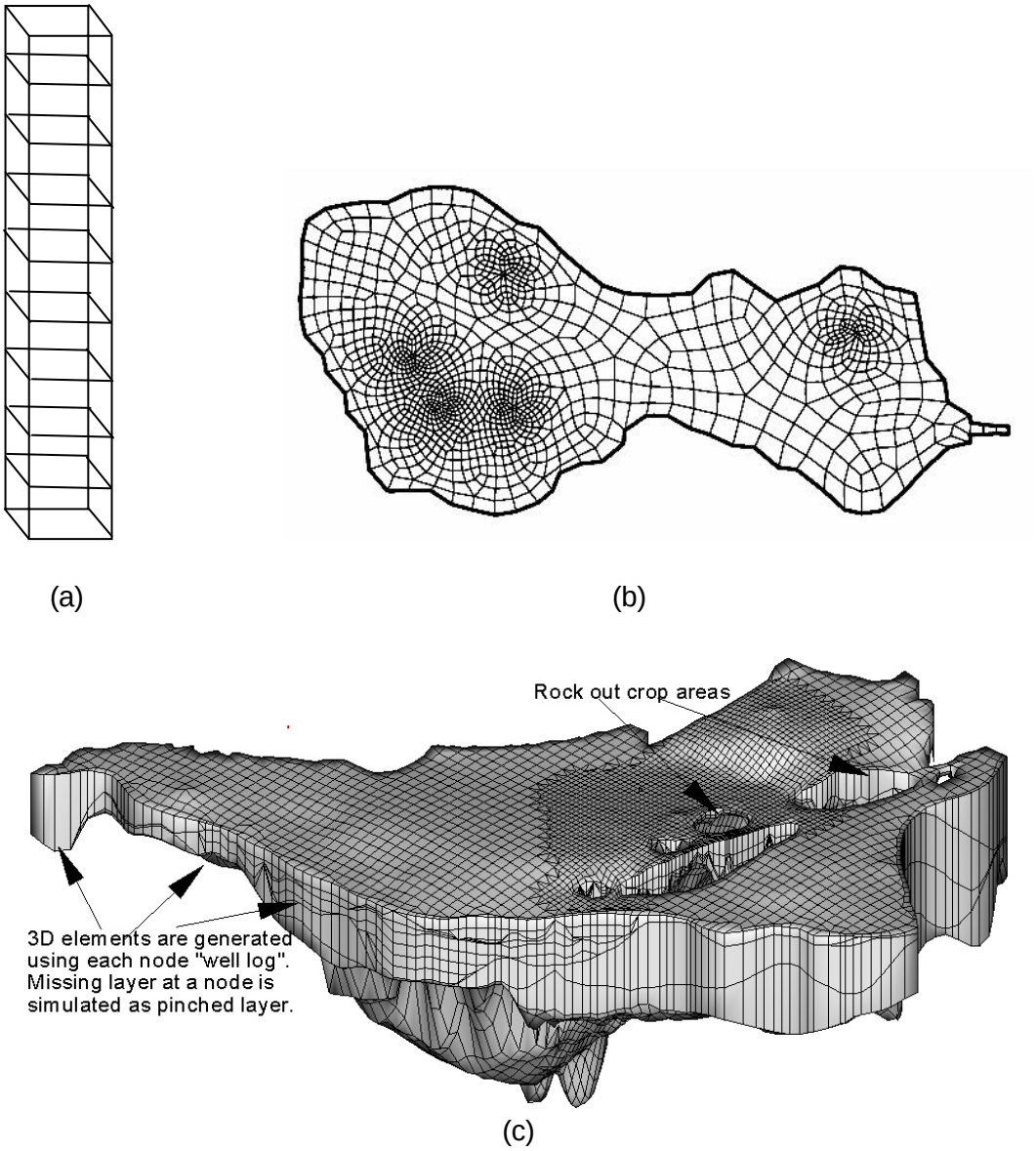

Figure 3.2. Examples of Arbitrary Hexahedral Meshes for (a) 1-D, (b) 2-D (third spatial dimension as a unit depth not shown), and (c) 3-D Finite Element Simulations

3.1.3 3-D Mesh Construction from a 2-D Topology

Developing 3-D finite element mesh models for irregular geometric objects can require a large amount of manual effort, which can limit the use of a 3-D approach for solving groundwater problems. CFEST simplifies this process by providing an automatic procedure that can be used to generate a 3-D finite element mesh from a 2-D quadrilateral surface grid.

Unlike other approaches, the technique used in CFEST incorporates information about the subsurface geometry with the quadrilateral surface topology to convert surface elements to spatial elements. This is accomplished by providing a well log with the top and bottom elevations of each layer (or material type) at each node. Subsurface nodes are generated in the problem domain for each data point in the well log. Once nodes are generated with depth, hexahedral orthogonal curvilinear elements are formed. Hence, the vertical mesh size is based on the thickness of the material described in each of the well logs. To create thinner elements, additional data points are required in the well logs, although no changes may occur in the stratigraphy.

Node numbers beneath the surface are assigned by adding to the surface node, the product of the layer number times the maximum number of surface nodes (100,000). As CFEST converts the 2-D surface grid to a 3-D hexahedral finite element grid, the additional subsurface nodes are numbered as

$$NN_{subsurface} = NN_{surface} + MN * 100000 \tag{3.1}$$

where $NN_{subsurface}$ is the node number for the additional subsurface node, $NN_{surface}$ is the surface node number, and MN is the material type or layer number defined by an integer in the well log. For example, material type number 3 beneath node 10 in the surface grid would be assigned a node number of 300,010 (i.e., 10 + 3*100,000 = 300,010). Subsurface element numbers are assigned in a similar manner.

3.2 Galerkin Finite Element Formulation

The standard Galerkin finite element scheme (e.g., Huyakorn and Pinder 1983) is applied to obtain the numerical solution of the governing equations. The Galerkin method is based on a weighted residual principle that states that the residual at each point in the problem domain is a measure of the extent to which the solution of the primary variable (e.g., pressure, concentration, or temperature) does not satisfy the governing equation. If the weighted average of the residual is forced to zero, the solution of the system of algebraic equations is obtained for the primary variable(s).

In the sections that follow, the application of Galerkin's method to the governing equation for flow is presented in detail. Because the same method is applied to the governing equations for mass transport and heat transfer, only the final discretized governing equations are presented for these equations. The relevant details for the Galerkin method include writing the governing equations in operator form and defining an approximate or trial solution for the primary variable expressed as a series summation. This summation is defined as the product of the primary variable and its basis function at each node in the problem domain. Integration of each of the terms proceeds based on the type of interpolation that must be performed.

3.2.1 Discretization of the Flow Equation

To apply Galerkin's method to the equation for variable density flow, Eq. (2.22) can be written as

$$L(P) = \left[\left(\alpha \rho \theta_o \right) \frac{\partial P}{\partial t} + \rho_o \theta \frac{\partial \Gamma}{\partial t} \right] + \nabla \cdot \rho \left[\frac{-k}{\mu} \left(\nabla P + \rho g \nabla z \right) \right] - \Omega = 0 \tag{3.2}$$

where L(P) represents the operator form of the continuity equation for momentum. In Eq. (3.2), material properties (e.g., permeability, porous media compressibility) are assigned by elements, whereas other terms, such as pressure and elevation, are described at the nodes. This results in an inexact description of the derivatives and variables where Eq. (3.2) does not equal exactly zero but a residual ε given as

$$\varepsilon = \left[(\alpha\rho\theta_o)\frac{\partial P}{\partial t} + \rho_o\theta\frac{\partial \Gamma}{\partial t} \right] + \nabla \cdot \rho\left[\frac{-k}{\mu}(\nabla P + \rho g \nabla z) \right] - \Omega \tag{3.3}$$

The residual ε is the result of approximating the terms of Eq. (3.2) and must be kept small everywhere in the problem domain to approximate the solution of the governing equation.

Solution of Eq. (3.3) by the Galerkin finite element technique requires the definition of a set of approximate or trial solutions given as

$$P(x_i,t) \approx \hat{P}(x_i,t) = \sum_{j=1}^{N} P(t)_j \phi_j(x_i) \tag{3.4a}$$

$$C(x_i,t) \approx \hat{C}(x_i,t) = \sum_{j=1}^{N} C(t)_j \phi_j(x_i) \tag{3.4b}$$

$$T(x_i,t) \approx \hat{T}(x_i,t) = \sum_{j=1}^{N} T(t)_j \phi_j(x_i) \tag{3.4c}$$

where $\hat{P}$, $\hat{C}$ and $\hat{T}$ are approximate solutions, and P_j, C_j and T_j are the nodal values of pressure, concentration, and temperature, respectively, at node *j*. *N* represents the total number of nodes in the finite element mesh, ϕ_j represents the global basis functions, and x_i ($i = 1, 2, 3$) is the spatial coordinates. In the following, the dependence of the primary variables on x_i and *t* has been eliminated for clarity.

In the standard Galerkin finite element scheme, the weighting functions (ϕ_i) are identical to the global basis functions. Upon substitution of the approximate solution, the weighted residual integral is constructed of the form:

$$\int_V \varepsilon\phi_i dV = 0 \qquad\qquad i = 1,\ldots,N \tag{3.5}$$

A system of algebraic equations is obtained by subdividing the above integral over the porous matrix domain *V* into piecewise elemental contributions of volume V^e. These steps are outlined in the sections that follow.

3.2.1.1 Time and Source Discretization

Time discretization in CFEST is based on a finite difference representation of cells. Thus, the first term in Eq. (3.2) is expanded by approximating the time derivative by a finite difference representation. Using the approximate solutions given in Eq. (3.4), the contribution at node *j* for the time derivative is then given as

$$\int_V \phi_i \left[(\alpha\rho\theta_o)\frac{\partial P}{\partial t} + \rho_o\theta\frac{\partial \Gamma}{\partial t} \right] dV = \int_V \phi_i \sum_{j=1}^{N} \phi_j \left[(\alpha\rho\theta_o)\left(\frac{P_j^{L+1} - P_j^L}{\Delta t} \right) + \rho_o\theta\left(\frac{\Gamma_j^{L+1} - \Gamma_j^L}{\Delta t} \right) \right] dV \tag{3.6}$$

where *V* is the region or control volume associated with node *j*, *L* is the time level, and Δt is time step size. Here, a fully implicit discretization in time is used.

Likewise, the source term in Eq. (3.3) is defined as the volume of fluid entering at node *j* and is associated with zero-order derivative terms. Hence, only the basis functions appear in the source term integral for the region *V*:

$$\int_V \phi_i \Omega dV = \int_V \phi_i \sum_{j=1}^{N} \Omega_j \phi_j dV \tag{3.7}$$

3.2.1.2 Application of Green's Theorem

The second term on the left side of Eq. (3.2) contains the primary variable for pressure and needs to be expressed as a function of the total pressure difference between node *i* and each of its neighbors. This is accomplished by applying Green's theorem (integration by parts), which converts the integral into two terms, one that is evaluated over the entire volume and the other at the region's surface:

$$\int_V \phi_i \left\{ \nabla \cdot \rho \left[\frac{-k}{\mu} (\nabla P + \rho g \nabla z) \right] \right\} dV = \int_V \frac{\rho k}{\mu} [\nabla P + \rho g \nabla z] \nabla \phi_i dV - \int_B \phi_i n \bullet \frac{\rho k}{\mu} [\nabla P + \rho g \nabla z] dB = \int_V \frac{\rho k}{\mu} [\nabla P + \rho g \nabla z] \nabla \phi_i dV - \int_B \phi_i n \bullet q^* dB \tag{3.8}$$

where q^* [m s^{-1}] is the Darcy flux at the boundary, and n is the surface vector normal to Darcy flux. The last term on the right side of Eq. (3.8) is proportional to the fluid flux normal to the boundary, *B*, of volume, *V*, weighted by ϕ_i at the boundary points.

Substitution of Eq. (3.4a) into the first term of Eq. (3.8) yields

$$\int_V \frac{\rho k}{\mu}\left[\nabla \hat{P} + \rho g \nabla z\right]\nabla \phi_i dV = \int_V \frac{\rho k}{\mu}\left(\sum_{j=1}^{N} P_j{}^{L+1}\nabla \phi_j + \rho g \nabla z\right)\nabla \phi_i dV \tag{3.9}$$

Both the pressure and gravity-elevation terms are weighted by the derivatives of the same weighting function, ϕ_i. This ensures that consistent nodal values of pressure and density will be obtained (Voss and Souza 1984).

3.2.1.3 Final Form of Discretized Flow Equation

By combining Eq. (3.6), (3.7), (3.8) and (3.9) and assuming a fully implicit method for discretization in time, the final form of the discretized equation for all of the elemental contributions for each element is obtained:

$$\begin{aligned}
&\sum_{j=1}^{N}\left\{\int_V \phi_i\phi_j\left[\left(\alpha\rho\theta_o\right)\left(\frac{P_j^{L+1}-P_j^{L}}{\Delta t}\right)+\rho_o\theta\left(\frac{\hat{\Gamma}_j^{L+1}-\hat{\Gamma}_j^{L}}{\Delta t}\right)\right]\right.\\
&+\int_V \frac{\rho k}{\mu}P_j{}^{L+1}\nabla\phi_j\nabla\phi_i dV+\int_V \frac{\rho k}{\mu}\rho g\nabla z\nabla\phi_i dV-\int_B \phi_i n\bullet q^* dB\\
&\left.-\int_V \phi_i\left[\left(\Omega_{in}+P_{j_{in}}^{L}\frac{d\Omega_{in}}{dP}\right)+\left(\Omega_{out}+P_{j_{out}}^{L}\frac{d\Omega_{out}}{dP}\right)\right]dV\right\}=0\\
&\qquad\qquad\qquad\qquad\qquad\qquad\qquad\qquad i,\ j=1,\ldots N
\end{aligned} \tag{3.10}$$

Hence, N algebraic equations are obtained for the pressure head distribution for each node *j* in the finite element grid.

The integrals over each element in Eq. (3.10) are evaluated numerically using Gaussian quadrature (e.g., Pinder and Gray 1977). This is accomplished by approximating the integrals in Eq. (3.10) by a sum of weights times the integrand values. In CFEST, a three-point Gaussian quadrature rule is used. The details of this method are given in Section 3.6.

3.2.1.4 Matrix Solution

The N algebraic equations given in Eq. (3.10) may be rearranged and rewritten in general matrix form:

$$[G]\{P\}+[S]\left\{\frac{\partial P}{\partial t}\right\}+[B]+[C]=\{F\} \tag{3.11}$$

where [G] is the conductance matrix, {P} is a column matrix of nodal pressures, [S] is a square matrix accounting for storage, $\{\partial P/\partial t\}$ is a column matrix of the time derivatives, [B] is the matrix for the elevation term in hydraulic head, [C] is the matrix of density derivatives term, and the {F} matrix is a column matrix

representing boundary conditions and the sink source term. These matrixes are defined as the sum of their elemental matrixes:

$$[G] = \sum_{e=1}^{m} [G]^e \tag{3.12a}$$

$$[S] = \sum_{e=1}^{m} [S]^e \tag{3.12b}$$

$$[B] = \sum_{e=1}^{m} [B]^e \tag{3.12c}$$

$$[C] = \sum_{e=1}^{m} [C]^e \tag{3.12d}$$

$$\{F\} = \sum_{e=1}^{m} \{F\}^e \tag{3.12e}$$

where typical elements of matrixes $[G]^e$, $[D]^e$, $[S]^e$, $[B]^e$, $[C]^e$, and $\{F\}^e$ are given by

$$G_{ij}^e = \int_V \frac{\rho k}{\mu} \nabla \phi_i^e \nabla \phi_j^e dV \tag{3.13a}$$

$$S_{ij}^e = \int_V \phi_i^e \phi_j^e \left(\alpha \rho \theta_o \right) dV \tag{3.13b}$$

$$B_{ij}^e = \int_V \frac{\rho k}{\mu} \rho g \nabla z \nabla \phi_i^e dV \tag{3.13c}$$

$$C_{ij}^e = \int_V \rho_o \theta \left(\frac{\hat{\Gamma}_j^{L+1} - \hat{\Gamma}_j^L}{\Delta t} \right) dV \tag{3.13d}$$

$$F_i^e = \int_V \phi_i^e \left[\begin{array}{l} \left(\Omega_{in} + P_{j_{in}}^L \frac{d\Omega_{in}}{dP} \right) + \\ \left(\Omega_{out} + P_{j_{out}}^L \frac{d\Omega_{out}}{dP} \right) \end{array} \right] dV + \int_B \phi_i^e n \bullet q^* dB \tag{3.13e}$$

The subdivision of the problem domain into elements means that the integrals are evaluated for each element, and the nodal basis functions (ϕ_j^e) are nonzero only for the elements that include node *j*. The eight nodes for each hexahedral element in the problem domain yield element conductance matrixes, [G^e], that contain eight rows and eight columns. The individual terms of [G^e] are found by evaluating Eq. (3.13a). The element contributions are then computed, dispersed, and summed to form the global conductance matrix given in Eq. (3.12a).

3.2.2 Discretization of the Solute Transport Equation

The solute transport equation is discretized in a manner similar to the flow equation. Applying the Galerkin method to the equation for solute mass transport, Eq. (2.22) is expanded and rewritten in operator form:

$$\begin{aligned} L(C) = &-\nabla\cdot(\theta\rho \mathrm{D}\nabla C) + \nabla(\rho q C) + \theta\rho C\lambda\left(1+\frac{\rho_b K_d}{\theta}\right) \\ &+\left[(\rho C)\alpha\theta_o\frac{\partial P}{\partial t} + (\rho_0\theta C)\frac{\partial \Gamma}{\partial t} + (\rho\theta)\frac{\partial C}{\partial t}\right]\left(1+\frac{\rho_b K_d}{\theta}\right) - \Omega_c \end{aligned} \tag{3.14}$$

Using the trial solutions defined in Eq. (3.4), Green's theorem for the dispersive term, and approximating the time derivative by finite difference, the finite element formulation for the solute transport equation is given:

$$\begin{aligned} &\sum_{j=1}^{N}\left\{\int_V \phi_i\phi_j\left[\left(\rho C_j^{\,L+1}\right)\alpha\theta_o\left(\frac{\hat{P}_j^{\,L+1}-\hat{P}_j^{\,L}}{\Delta t}\right)+\left(\rho_0\theta C_j^{\,L+1}\right)\left(\frac{\hat{\Gamma}_j^{\,L+1}-\hat{\Gamma}_j^{\,L}}{\Delta t}\right)\right.\right. \\ &\left.+(\rho\theta)\left(\frac{C_j^{\,L+1}-C_j^{\,L}}{\Delta t}\right)\right]\left(1+\frac{\rho_b K_d}{\theta}\right)dV \\ &+\int_V \nabla\cdot\phi_i\left(\theta\rho \mathrm{D} C_j^{L+1}\nabla\phi_j\right)dV - \int_B\left(\phi_i n\bullet\theta\rho\mathrm{D}\nabla C\right)dB \\ &-\int_V \nabla\cdot\phi_i\phi_j\rho q C_j^{L+1}\,dV + \int_B\left(\phi_i n\bullet\rho q C\right)dB \\ &\left.+\int_V \phi_i\phi_j\theta\rho C_j^{L+1}\lambda\left(1+\frac{\rho_b K_d}{\theta}\right) - \int_V \phi_i\Omega_c\,dV\right\} = 0 \\ &\qquad\qquad i,\, j = 1,\ldots N \end{aligned} \tag{3.15}$$

where the first integral term represents the time derivative, the second integral the diffusive-dispersive flux, and the third integral the diffusive flux normal to the boundary. The fourth integral in Eq. (3.15) represents the advective flux, the fifth is the advective flux normal to the boundary, the sixth is the concentration changes due to decay, and the last integral is the sink/source term. The N algebraic equations can be arranged and written in general matrix form:

$$\left(\left[A\right]+\left[D\right]+\left[K\right]+\left[E\right]\right)\{C\}+[M]\left\{\frac{\partial C}{\partial t}\right\}=\{F\} \tag{3.16}$$

where [A] is the advection matrix, [D] is the dispersion matrix, [K] is the sorption matrix, [E] is the matrix of concentration due to the pressure and density change, {C} is a column matrix of nodal concentrations, [M] is the mass matrix associated with the time derivative terms, and $\{\partial C/\partial t\}$ is a column matrix of the time derivatives. Like the column matrix {F} in Eq. (3.11), the {F} vector represents contributions from sinks, sources, and boundary conditions. These matrixes are defined as the sum of their elemental matrixes, given as

$$\left[A\right]=\sum_{e=1}^{m}\left[A\right]^{e} \tag{3.17a}$$

$$\left[D\right]=\sum_{e=1}^{m}\left[D\right]^{e} \tag{3.17b}$$

$$\left[K\right]=\sum_{e=1}^{m}\left[K\right]^{e} \tag{3.17c}$$

$$\left[E\right]=\sum_{e=1}^{m}\left[E\right]^{e} \tag{3.17d}$$

$$\left[M\right]=\sum_{e=1}^{m}\left[M\right]^{e} \tag{3.17e}$$

$$\{F\}=\sum_{e=1}^{m}\{F\}^{e} \tag{3.17f}$$

where typical elements of matrixes $[A]^e$, $[D]^e$, $[K]^e$, $[M]^e$, and $\{F\}^e$ are given by

$$A_{ij}^{e}=-\int_{V}\nabla\cdot\phi_{i}^{e}\phi_{j}^{e}\rho q dV \tag{3.18a}$$

$$D_{ij}^{e}=\int_{V}\nabla\cdot\phi_{i}^{e}\left(\theta\rho\mathrm{D}\nabla\phi_{j}^{e}\right)dV \tag{3.18b}$$

$$K_{ij}^{e}=\int_{V}\phi_{i}^{e}\phi_{j}^{e}\theta\rho\lambda\left(1+\frac{\rho_{b}K_{d}}{\theta}\right)dV \tag{3.18c}$$

$$E_{ij}^{e} = \int_{V} \phi_i^{e} \phi_j^{e} \left[\left(\rho \alpha \theta_o \right) \left(\frac{\hat{P}_j^{L+1} - \hat{P}_j^{L}}{\Delta t} \right) + \left(\rho_0 \theta \right) \left(\frac{\hat{\Gamma}_j^{L+1} - \hat{\Gamma}_j^{L}}{\Delta t} \right) \right] \left(1 + \frac{\rho_b K_d}{\theta} \right) dV \tag{3.18d}$$

$$M_{ij}^{e} = \int_{V} \phi_i^{e} \phi_j^{e} \rho \theta \left(1 + \frac{\rho_b K_d}{\theta} \right) dV \tag{3.18e}$$

$$F_i^{e} = \int_{B} \left(\phi_i^{e} n \bullet \theta \rho \mathrm{D} \nabla C \right) dB + \int_{V} \phi_i^{e} \Omega_c \, dV - \int_{B} \left(\phi_i^{e} n \bullet \rho q C \right) dB \tag{3.18f}$$

3.2.3 Discretization of the Heat Transfer Equation

The heat transfer equation is also discretized by applying the Galerkin method to the equation for solute mass transport. Combining Eq. (2.34) and (2.35) for the time derivative expressed in Eq. (2.29), the governing equation for heat transfer in operator form is written as

$$\begin{aligned} L(T) = {} & \nabla \theta \kappa \left(\nabla T \right) - \nabla T \cdot \theta \rho q c_p - \\ & \left\{ \begin{array}{l} \left(\alpha \theta_o T \right) \left[c_p \rho - c_s \rho_b \right] \dfrac{\partial P}{\partial t} + \\ \theta c_p T \dfrac{\partial \Gamma}{\partial t} + \left[c_p \rho \theta + c_s \rho_b - c_s \rho_b \theta \right] \dfrac{\partial T}{\partial t} \end{array} \right\} + \Omega_T \end{aligned} \tag{3.19}$$

Using the trial solutions defined in Eq. (3.4), Green's theorem for the dispersive term, and approximating the time derivative by finite difference, the finite element formulation for the heat transfer equation is given as

$$\begin{aligned} & \sum_{e=1}^{m} \left\{ \int_{V} \phi_i \phi_j \left[\left(\alpha \theta_o T_j^{L+1} \right) \left[c_p \rho - c_s \rho_b \right] \left(\frac{\hat{P}_j^{L+1} - \hat{P}_j^{L}}{\Delta t} \right) \right. \right. \\ & + \left(\frac{T_j^{L+1} - T_j^{L}}{\Delta t} \right) \left[c_p \rho \theta + c_s \rho_b - c_s \rho_b \theta \right] \\ & \left. + \theta c_p T_j^{L+1} \frac{\hat{\Gamma}_j^{L+1} - \hat{\Gamma}_j^{L}}{\Delta t} \right] dV \Bigg] \\ & - \int_{V} \nabla \phi_i \left(\nabla \phi_j \theta \kappa T_j^{L+1} \right) dV + \int_{B} \left(\phi_i \theta \kappa \nabla T \bullet n \right) dB \\ & \left. - \int_{V} \phi_i \nabla \phi_j \theta \rho q c_p T_j^{L+1} dV + \int_{V} \phi_i \Omega_T dV \right\} = 0 \end{aligned} \tag{3.20}$$

$$i, \, j = 1, \ldots N$$

The first integral term, which spans the first three lines of the equation, represents the time derivative. The second integral is the diffusive-dispersive flux, and the third is the heat conduction and thermal dispersion normal to the boundary. The fourth integral in Eq. (3.20) represents the heat transfer by convection, and the fifth is a heterogeneous thermal source/sink term. The N algebraic equations can be arranged and written in general matrix form:

$$\left(\left[A\right]+\left[D\right]+\left[E\right]\right)\left\{T\right\}+\left[M\right]\left\{\frac{\partial T}{\partial t}\right\}=\left\{F\right\} \tag{3.21}$$

where [A] is the convection matrix, [D] is the conduction/diffusivity matrix, [E] is the matrix of temperature due to pressure and density change, {T} is a column matrix of nodal temperatures, [M] is the matrix associated with the time derivative terms, and $\left\{\partial T/\partial t\right\}$ is a column matrix of the time derivatives. Similar to the other vectors formed by the discretization of the governing equations, the {F} vector represents contributions from sinks, sources, and boundary conditions. These matrixes are defined as the sum of their elemental matrixes given as

$$\left[A\right]=\sum_{e=1}^{m}\left[A\right]^{e} \tag{3.22a}$$

$$\left[D\right]=\sum_{e=1}^{m}\left[D\right]^{e} \tag{3.22b}$$

$$\left[M\right]=\sum_{e=1}^{m}\left[M\right]^{e} \tag{3.22c}$$

$$\left\{F\right\}=\sum_{e=1}^{m}\left\{F\right\}^{e} \tag{3.22d}$$

where typical elements of matrixes $[A]^e$, $[D]^e$, $[M]^e$ and $\{F\}^e$ are given by

$$A_{ij}^{e}=-\int_{V}\phi_i^{\,e}\nabla\phi_j^{\,e}\theta\rho qc_p\;\;dV \tag{3.23a}$$

$$D_{ij}^{e}=-\int_{V}\nabla\phi_i^{\,e}\left(\nabla\phi_j^{\,e}\theta\kappa\right)dV \tag{3.23b}$$

$$M_{ij}^{e}=\int_{V}\phi_i^{e}\phi_j^{\,e}\left(c_p\rho\theta+c_s\rho_b-c_s\rho_b\theta\right)dV \tag{3.23c}$$

$$E_{ij}^{e}=\int_{V}\phi_i\phi_j\left[\left(\alpha\theta_o\right)\left[c_p\rho-c_s\rho_b\right]\left(\frac{\hat{P}_j^{\,L+1}-\hat{P}_j^{\,L}}{\Delta t}\right)+\left(\theta c_p\right)\left(\frac{\hat{\Gamma}_j^{\,L+1}-\hat{\Gamma}_j^{\,L}}{\Delta t}\right)\right]dV \tag{3.23d}$$

$$F_i^e = -\int_B \left(\phi_i^e \theta \kappa \nabla T \bullet n \right) dB - \int_V \phi_i^e \Omega_T \, dV \tag{3.23e}$$

3.2.4 Boundary Conditions

In CFEST, boundary conditions can be time variant and of the first type (Dirichlet), second type (Neumann), or third type (Cauchy). Free surface boundary conditions for unconfined aquifers and seepage face boundaries can also be implemented in CFEST.

All boundary conditions are incorporated into the boundary integral terms, which are proportional to a weighted average of the normal flux. For interior nodes, the weighting function in the boundary integral is zero; hence, the entire term is equal to zero. Likewise, at the boundaries, if a no-flux boundary is specified, the boundary integral term is zero and does not contribute to the entry in the elemental column vector {F}.

For specified flux conditions, the total flux on the boundary is given. For the flow equation, this involves specifying a Darcy flux that is entered directly into the column vector {F}. The pressure equation is then solved subject to the flux boundary condition. A similar treatment is considered for diffusive solute and heat flux boundaries. Advective fluxes for heat and solute transport are treated in their respective source terms.

For boundary nodes with fixed primary variables, the equations associated with these nodes are not necessary because the value of the primary value is already known. Therefore, in CFEST, specified (or Dirichlet) boundary conditions lead to a reduction in the number of unknowns and thereby the number of equations. However, the specified values of pressure, concentration, and/or temperature are used when they appear in any other equations.

Cauchy boundary conditions are a function of the primary variable, and a flux is computed given the boundary value of the dependent variable (e.g., pressure, concentration, or temperature). Hence, the specification of a Cauchy boundary condition results in a non-zero boundary integral and a corresponding entry in the {F} vector.

3.3 Basis and Weighting Functions

Using the finite element method requires that the equations be split into a number of subintegrals over individual elements and that these integrals be approximately computed using an appropriate quadrature scheme. To obtain these integrals, curved isoparametric transformation of the global coordinates to non-dimensional local coordinates is first carried out using shape functions in a scheme described by Zienkiewicz and Taylor (2000). The method can be thought of as the transformation of the arbitrary hexahedron from the finite element grid to a simple 3-D cube (Figure 3.3). The simple cube is defined in a local coordinate system (ξ_j, η_j, ζ_j) for $-1 \le \xi_j, \eta_j, \zeta \le 1$. When moving from local to global coordinates, the transformation results in the required Cartesian coordinates of the element in the finite element grid.

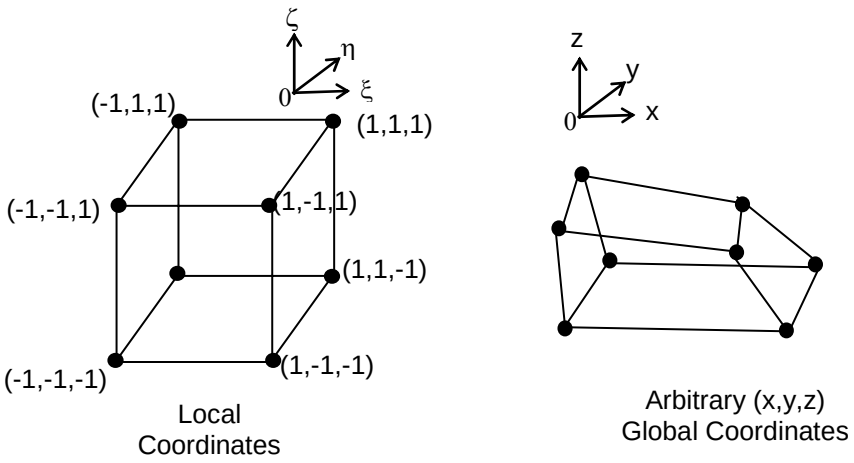

Figure 3.3. Isoparametric Elements in Global and Local Coordinates

To evaluate important element tensors, the strain-displacement transformations need to be calculated. These are obtained in terms of derivatives of element displacements with respect to the local coordinate system. Because the element displacements are defined in the local coordinate system, local derivatives need to be related to the global ones. These operations are carried out using the basis functions to linearly remap the coordinates in each coordinate direction. The basis function ϕ_j, defined for node *j*, has a value of one at the node and zero at the other nodes. It varies linearly along the straight element edges that connect node *j* to its neighbors. The basis functions in CFEST are defined as

$$\phi_1 = \frac{1}{8}(1-\xi)(1-\eta)(1-\zeta) \tag{3.24a}$$

$$\phi_2 = \frac{1}{8}(1+\xi)(1-\eta)(1-\zeta) \tag{3.24b}$$

$$\phi_3 = \frac{1}{8}(1+\xi)(1+\eta)(1-\zeta) \tag{3.24c}$$

$$\phi_4 = \frac{1}{8}(1-\xi)(1+\eta)(1-\zeta) \tag{3.24d}$$

$$\phi_5 = \frac{1}{8}(1-\xi)(1-\eta)(1+\zeta) \tag{3.24e}$$

$$\phi_6 = \frac{1}{8}(1+\xi)(1-\eta)(1+\zeta) \tag{3.24f}$$

$$\phi_7 = \frac{1}{8}(1+\xi)(1+\eta)(1+\zeta) \tag{3.24g}$$

$$\phi_8 = \frac{1}{8}(1-\xi)(1+\eta)(1+\zeta) \tag{3.24h}$$

The remapping of coordinates from global system to local system is given as

$$\begin{Bmatrix} x \\ y \\ z \end{Bmatrix} = \begin{Bmatrix} \sum \phi_i x_i \\ \sum \phi_i y_i \\ \sum \phi_i z_i \end{Bmatrix} \tag{3.25}$$

and the derivatives of basis functions can be derived as

$$\begin{Bmatrix} \frac{\partial \phi_i}{\partial \xi} \\ \frac{\partial \phi_i}{\partial \eta} \\ \frac{\partial \phi_i}{\partial \zeta} \end{Bmatrix} = \begin{bmatrix} \frac{\partial x}{\partial \xi} & \frac{\partial y}{\partial \xi} & \frac{\partial z}{\partial \xi} \\ \frac{\partial x}{\partial \eta} & \frac{\partial y}{\partial \eta} & \frac{\partial z}{\partial \eta} \\ \frac{\partial x}{\partial \zeta} & \frac{\partial y}{\partial \zeta} & \frac{\partial z}{\partial \zeta} \end{bmatrix} \begin{Bmatrix} \frac{\partial \phi_i}{\partial x} \\ \frac{\partial \phi_i}{\partial y} \\ \frac{\partial \phi_i}{\partial z} \end{Bmatrix} \tag{3.26}$$

The Jacobian matrix [J] of the derivative basis functions are calculated for each element:

$$[J] = \begin{bmatrix} \frac{\partial \phi_1}{\partial \xi} & \frac{\partial \phi_2}{\partial \xi} & \frac{\partial \phi_3}{\partial \xi} & \frac{\partial \phi_4}{\partial \xi} & \frac{\partial \phi_5}{\partial \xi} & \frac{\partial \phi_6}{\partial \xi} & \frac{\partial \phi_7}{\partial \xi} & \frac{\partial \phi_8}{\partial \xi} \\ \frac{\partial \phi_1}{\partial \eta} & \frac{\partial \phi_2}{\partial \eta} & \frac{\partial \phi_3}{\partial \eta} & \frac{\partial \phi_4}{\partial \eta} & \frac{\partial \phi_5}{\partial \eta} & \frac{\partial \phi_6}{\partial \eta} & \frac{\partial \phi_7}{\partial \eta} & \frac{\partial \phi_8}{\partial \eta} \\ \frac{\partial \phi_1}{\partial \zeta} & \frac{\partial \phi_2}{\partial \zeta} & \frac{\partial \phi_3}{\partial \zeta} & \frac{\partial \phi_4}{\partial \zeta} & \frac{\partial \phi_5}{\partial \zeta} & \frac{\partial \phi_6}{\partial \zeta} & \frac{\partial \phi_7}{\partial \zeta} & \frac{\partial \phi_8}{\partial \zeta} \end{bmatrix} \begin{bmatrix} x_1 & y_1 & z_1 \\ x_2 & y_2 & z_2 \\ x_3 & y_3 & z_3 \\ x_4 & y_4 & z_4 \\ x_5 & y_5 & z_5 \\ x_6 & y_6 & z_6 \\ x_7 & y_7 & z_7 \\ x_8 & y_8 & z_8 \end{bmatrix} \tag{3.27}$$

where the numbered subscripts refer to local element numbering for each of the eight vertices in the hexahedron (e.g., Figure 3.24). The Jacobian matrix [J] is used to transform the derivatives of the basis functions from the global to the local coordinate systems. However, the derivative of $\phi_j(x)$ cannot be determined directly with respect to *x* because it is not an explicit function of *x*. It is a function of ξ, which, in turn, is implicitly a function of *x* via the coordinate transformation. Using the chain rule of differentiation and inverting [J], the global derivatives are obtained:

$$\begin{bmatrix} \frac{\partial \phi_k}{\partial x} \\ \frac{\partial \phi_k}{\partial y} \\ \frac{\partial \phi_k}{\partial z} \end{bmatrix} = \left[J^{-1}\right] \begin{bmatrix} \frac{\partial \phi_k}{\partial \xi} \\ \frac{\partial \phi_k}{\partial \eta} \\ \frac{\partial \phi_k}{\partial \zeta} \end{bmatrix} \tag{3.28}$$

Here J denotes the Jacobian matrix of (x, y, z) with respect to (ξ, η, ζ), whereas J^{-1} is the Jacobian matrix of (ξ, η, ζ) with respect to (x, y,z). The subscript k refers to any one of the eight nodes in the 3-D element. The inverse Jacobian is defined as

$$[J^{-1}] = \frac{1}{\det J} adj\, J \tag{3.29}$$

where "det J" denotes the matrix determinant of [J]. The symbol "*adj* A" denotes the adjoint (or adjugate) of a matrix A and is defined as the transpose of the cofactor matrix of [J].

In addition to transforming the derivative from global to local coordinates, the differential volume must also be changed. Hence, a relationship between the volume integration in physical (global) coordinates and the volume integration in computational (local) coordinates can then be written in terms of the Jacobian determinant:

$$dV = dx\, dy\, dz = \left(\det J\right) d\xi\, d\eta\, d\zeta \tag{3.30}$$

Numerical Gaussian quadrature is then used to evaluate the integral of the function f by approximating the weighted sum of values of f at selected points. This is accomplished by approximating the integrals by a sum of weights times the integrand values. In CFEST, a two-point Gaussian quadrature rule is used:

$$\int_V f\left(\xi,\eta,\zeta\right) dV \approx \sum_{j=1}^{N} \omega_j f\left(\xi,\eta,\zeta\right)\left(\det J\right) \tag{3.31}$$

where ω_j are the weights associated with the quadrature points. Gaussian quadrature abscissae (coordinates) and weights used in CFEST are given in Zienkowicz and Taylor (2000).

3.4 Sequential Iteration

Nonlinearities arising from the coupled problems are treated by applying sequential iteration, where, for each time step flow, transport and/or heat transfer equations are solved sequentially until convergence is attained. If, for example, the fluid density at a node changes substantially because of changes in temperature or solute concentration, the fluid flow equation must be resolved for a new estimate of pressure or hydraulic head. Following solution of the fluid transport equation, new estimates must be made for the temperature and solute concentration distribution. Iterations are continued until the change in fluid density at each node is within a predefined tolerance. If the change in density over a time step is significant, iteration of the solute

transport and fluid flow equations is needed. This principle is used to test the convergence of density by distinguishing changes caused by temperature and solute. A tolerance of 0.001 is used to test convergence of density (ρ):

$$\frac{\Delta\rho_T + \Delta\rho_C}{\rho_o} \leq 0.001 \tag{3.32}$$

where $\Delta\rho_T$ represents the maximum change in density at any node due to temperature, and $\Delta\rho_C$ is the maximum change in density due to concentration. If Eq. (3.32) is not satisfied, the following convergence tests are performed:

$$\frac{\Delta\rho_T}{\rho_o} \leq 0.0005 \tag{3.33a}$$

$$\frac{\Delta\rho_C}{\rho_o} \leq 0.0005 \tag{3.33b}$$

If neither of these criteria is met, equations for all three variables (pressure, temperature, and concentration) are resolved for the given time step. If only Eq. (3.33a) is satisfied, subsequent iterations include only the head and concentration solutions until Eq. (3.33b) is satisfied. After convergence is obtained, the energy equation is solved. A similar procedure is used if Eq. (3.33b) is satisfied, but not Eq. (3.33a).

3.5 Linear System Solvers

The discretization of the governing partial differential equations in CFEST leads to the formation of a sparse linear system of equations in which most of the coefficients of the matrix are zero. Two solvers are implemented in CFEST for solving sparse matrixes, including the nonsymmetric preconditioned conjugate gradient (NSPCG) software package in ITPACK (Young and Kincaid 1981) and Portable, Extensible Toolkit for Scientific Computation (PETSc) (Balay et al. 2004). Both solvers solve nonsingular systems of the form A x = b, where A denotes the coefficient matrix, b is the right-side vector, and x is the solution vector. Elements within the A matrix are actually submatrixes, where the submatrix order equals the number of coupled governing equations. For example, if only the mass conservation of water is solved, single-element matrixes result. If both flow and solute transport are solved, then the submatrix order is two.

Both the ITPACK-NSPCG and PETSc solvers are implemented using iterative methods. These methods start with an initial guess of the solution, generate a sequence of approximations, and often only require matrix-vector multiplications and inner products. The power of most iterative methods is in how cheaply each solve may be performed. By contrast, the weakness of these methods is that several iterations may be required to arrive at a solution. This number can be reduced by preconditioning the matrix, but only at the expense of increasing the cost of each iteration. A good preconditioner sufficiently improves the convergence of the iterative method to overcome the extra cost of constructing and applying the preconditioner.

3.5.1 ITPACK

The ITPACK-NSPCG software package is used in the solution of the linear algebraic equations resulting from discretization of the governing equations. NSPCG software is publicly available and was developed at the Center for Numerical Analysis at The University of Texas at Austin for solving large sparse systems of linear algebraic equations. ITPACK matrix solver applies various accelerators and preconditioners in solving the matrix. For the banded matrix generated by the partial differential equations in CFEST, only the nonzero elements are stored, which significantly economizes computer memory usage.

NSPCG uses iterative methods such as conjugate gradients, successive over-relaxation, and Jacobi iteration in conjunction with various preconditioners. Basic preconditioners also included in NSPCG are Jacobi, incomplete LU decomposition, modified incomplete LU decomposition, and successive over-relaxation (SOR). Methods used for the nonsymmetric matrixes posed by the transport equations include ORTHOMIN, generalized conjugate residual (GCR), Lanczos, and LSQR. Detailed information on the iterative techniques and preconditioning methods may be found in Young and Kincaid (1981).

The iterative methods from ITPACK are implemented through direct calls to subroutines. The arguments in these calls pass the iterative method and the acceleration scheme desired, which are either set by default or by the user. If convergence is not achieved, CFEST implements an efficient procedure for cycling through different accelerators so that only the most efficient methods are used.

3.5.2 PETSc

The PETSc solver is also implemented in CFEST. PETSc, developed at Argonne National Laboratory (Balay et al. 2004), is a suite of data structures and routines for scalable (parallel) matrix solves. Although PETSc is intended for use with parallel, large-scale applications, it is also implemented in serial in CFEST. The parallel capability in CFEST only applies to the PETSc solver and can be used for the solution of the flow and solute transport equations.

Like the ITPACK-NSPCG solver, PETSc supports the compressed sparse row storage format. Although PETSc contains both direct and iterative linear solution methods, only the conjugate gradient and generalized minimal residual (gmres) iterative methods have been implemented in CFEST. In addition to the preconditioners cited as available in NSPCG, PETSc includes the incomplete LU and Cholesky methods as well as many others.

Unlike NSPCG, special data structures in PETSc are required. These are created in CFEST through function calls. Default options for the preconditioners are set within CFEST, but can be modified by the user upon execution of the code using command line arguments.

4.0 Verification Problems

The objective of this section is to verify whether the mathematical equations are solved accurately using the numerical methods outlined in this report. Eight distinct verification problems are presented that test different aspects of the CFEST simulator for both flow and solute transport. No heat transfer verification problems are presented because this module has not yet been fully implemented in CFEST.

In the following sections, CFEST numerical solutions are compared with known analytical solutions. For flow, the set of verification problems includes uniform steady-state flow, uniform transient flow, free-surface boundary (Boussinesq) with recharge, and free-surface boundary with a seepage face. For solute transport, the verification problems include transient 1-D diffusion, flux concentration boundary condition, and a held concentration boundary problem. For coupled solution, a seawater intrusion problem is solved for a density-dependent flow and solute transport problem.

4.1 Flow Verification

4.1.1 Uniform Steady-State Flow

The Theim equation (Bear 1979) is a mathematical expression that relates well discharge to drawdown and assumes 2-D radial flow toward a well. All dynamic conditions in the well and ground are assumed to be in equilibrium, and water enters the well in equal volumes from all directions. Drawdown resulting from these steady conditions is expressed as

$$s = \frac{Q}{2\pi Kb}\ln\left(R_o / R\right) \tag{4.1}$$

where s is the drawdown (L), Q is the volumetric flow rate (L^3t^{-1}), K is the aquifer hydraulic conductivity ($L\ t^{-1}$), b is the aquifer thickness (L), and R represents the radius of observation from the pumping well to the observation point (L), and R_o is the radius of influence (L).

Parameters used for both the analytical and CFEST solutions are shown in Table 4.1. Because of the symmetry of radial flow to a single pumping well, a pie-shaped wedge was constructed from finite elements. For CFEST, two separate simulations were run, distinguished by the model discretization. One grid used a uniform spacing of $\Delta R = 2$ m, and the other used a uniform spacing of $\Delta R = 0.5$ m for finite elements with the 11.25° segment angles (A) shown in Figure 4.1. These radial slices accounted for $^1/_{32}$ of the total area of influence. Figure 4.2 is a plot of the analytical and simulated results. Although the results for both ΔRs closely coincide, the more finely discretized grid ($\Delta R = 0.5$ m) resulted in drawdown estimates that were no more than 0.54% from the analytical solution. For $\Delta R = 2$ m, the largest discrepancy between the numerical and analytical solution was 1.87%.

Table 4.1. Parameter Values Used in the Uniform Steady-State Flow Problem

Parameters	Units	Value
Q	m^3/day	10
K	m/day	1
b	m	1
R_0	m	20

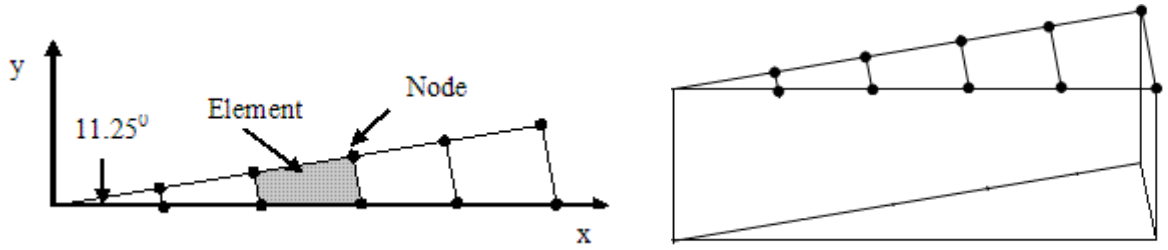

Figure 4.1. The 11.25° Segment Angle Element Shape and 3-D View

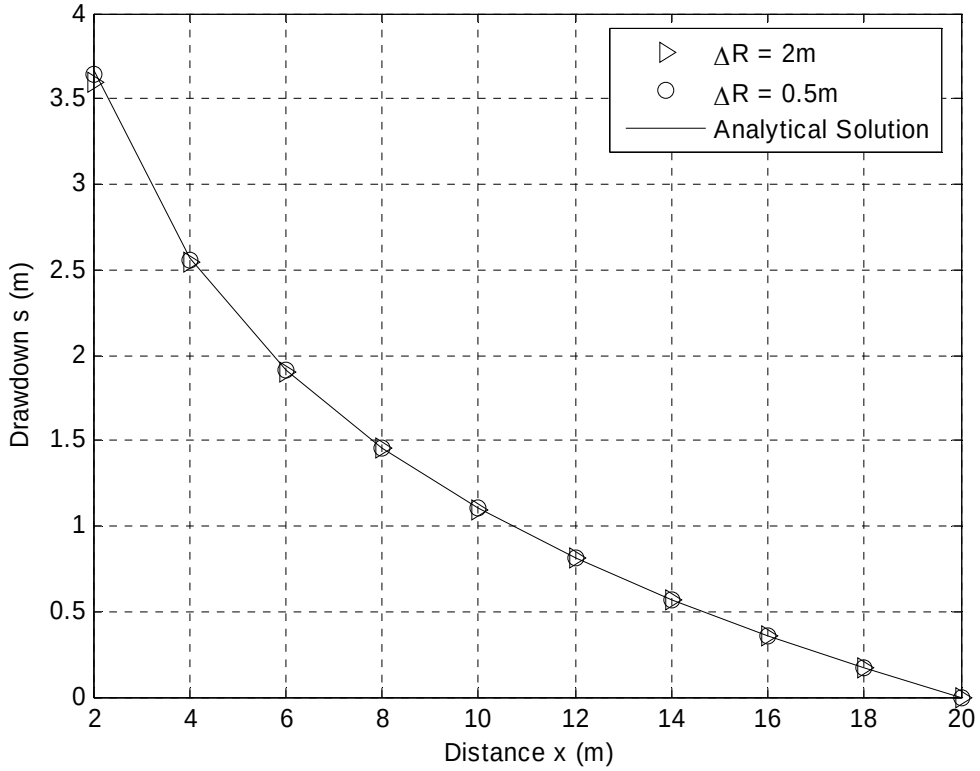

Figure 4.2. Analytical and Simulated Steady-State Drawdown in a Confined Aquifer

4.1.2 Nonequilibrium Flow

The Theis (1935) nonequilibrium well equation accounts for transient effects on well yield. Several assumptions were used to derive the Theis equation, including an isotropic aquifer of uniform thickness, a constant pumping rate, and an assumption that all water removed from storage comes from aquifer storage and is discharged instantaneously when the head is lowered. The Theis equation is given as

$$s = \frac{Q}{4\pi T}\int_{u}^{\infty}\frac{e^{-u}\,du}{u} \tag{4.2}$$

where T is the aquifer transmissivity [L^2t^{-1}], and u is the dimensionless well function defined as

$$u = \frac{R^2 S}{4Tt} \tag{4.3}$$

In Eq. (4.3), R represents the radial distance from the pumping well to the observation point [L], S is the dimensionless storage coefficient, and t is the pumping time.

Due to the symmetry of radial flow to a single pumping well, a pie-shaped wedge was constructed from finite elements with an angle A of 22.5°. A nonuniform grid spacing was used with progressively larger radial increments spaced by a geometric ratio of 1.414 at increasing distances from the well (Figure 4.3). This grid represented $^1/_{16}$ of the total area of influence and bounded the aquifer at a large distance from the well. Similarly, time steps for the numerical simulation were also increased using a geometric ratio of 2. The initial time step was 10^{-5} day, and the maximum time step was 0.1 day. In total, ~2.8 days were simulated over 40 time steps.

Parameters used for both solutions are shown in Table 4.2. Results of the CFEST and analytical solutions are shown in Figure 4.4. The plot of drawdown versus time shows excellent agreement for unsteady flow in a confined aquifer.

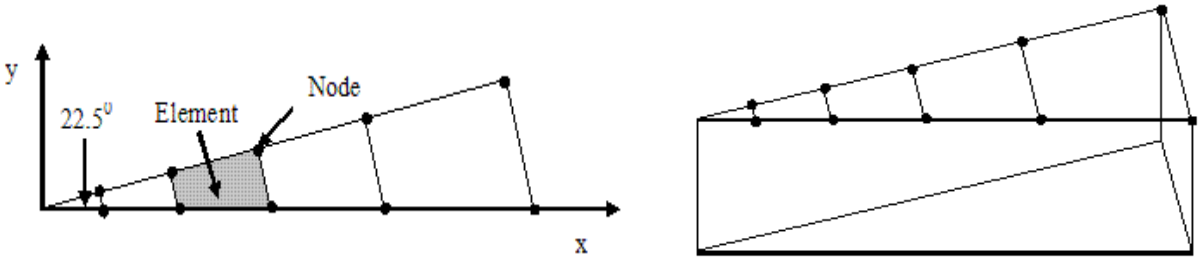

Figure 4.3. The 22.5° Segment Angle Element Shape with Exponentially Increasing $\Delta r_i = 1.414\Delta r_{i-1}$ and 3-D View

Table 4.2. Parameter Values Used in the Nonequilibrium Flow Problem

Parameters	Units	Value
Q	ft^3/day	7200
T	ft^2/day	100
S	dimensionless	0.001
R	ft	2

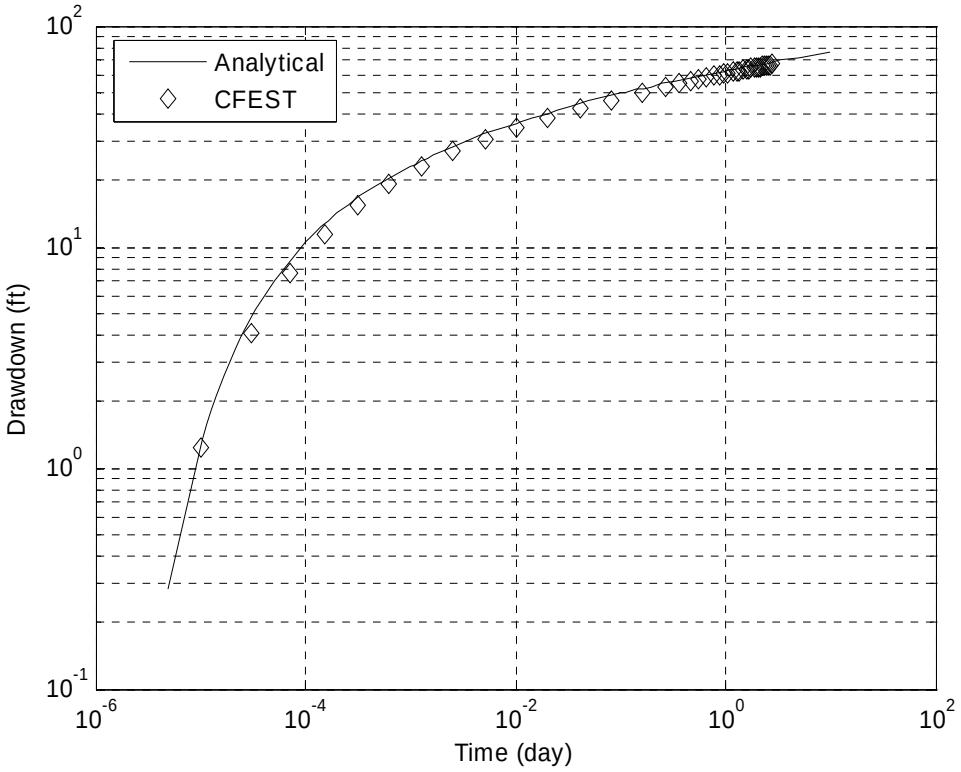

Figure 4.4. Theis (1935) and CFEST Solution of Time-Dependent Drawdown for a Well Pumped at a Constant Rate

4.1.3 Free-Surface Boussinesq Flow

If an aquifer is unconfined, its saturated thickness varies with the water table height. Under the Dupuit assumptions for 1-D flow through an unconfined aquifer, flow is horizontal and the hydraulic gradient is equal to the slope of the free surface. Hence, hydraulic head can be estimated by the Boussinesq equation for water flow in a phreatic aquifer as

$$K\frac{\partial}{\partial x}\left(h\frac{\partial h}{\partial x}\right)+\omega=\theta\frac{\partial h}{\partial t} \tag{4.4}$$

where ω represents vertical velocities, including recharge, infiltration and evaporation and the porosity, θ, is assumed to be equal to the specific yield (S_y). For the boundary conditions,

$$h(x,0) = h_2 \tag{4.5a}$$

and

$$h(0,t) = h_1 \tag{4.5b}$$

The analytical solution based on a power series approximation is given by Polubarinova-Kochina (1962). Ignoring any vertical leakage (ϖ), the analytical solution is expressed as

$$h = h_1\left(1 + lu_1 + l^2u_2 + l^3u_3 + \cdots\right) \tag{4.6}$$

where

$$l = \frac{h_2 - h_1}{h_1} \tag{4.7}$$

and the first approximation (u_1) is given as the probability function

$$u_1(\eta) = \phi(\eta) = \frac{2}{\sqrt{\pi}}\int_0^{\eta} e^{-\tau^2}\,d\tau \tag{4.8}$$

where η is defined as

$$\eta = \frac{x\sqrt{\theta}}{2\sqrt{Kh_1t}} \tag{4.9}$$

The second and third approximations are given by

$$u_2(\eta) = \frac{1}{\pi}\left(1 - e^{-2\eta^2}\right) - \frac{1}{\sqrt{\pi}}\eta e^{-\eta^2}u_1 - \frac{1}{2}u_1^3 + \left(\frac{1}{2} - \frac{1}{\pi}\right)u_1 \tag{4.10}$$

and

$$\begin{aligned} u_3(\eta) = {} & \left(\frac{1}{2}\right)u_1^3 + \left(\frac{9}{4\sqrt{\pi}}\eta e^{-\eta^2}\right)u_1^2 - \left(\frac{1}{2\sqrt{\pi}}\eta^3 e^{-\eta^2}\right)u_1^2 + \left(\frac{3}{\pi}e^{-\eta^2}\right)u_1 - \\ & \left(\frac{1}{\pi}\eta^2 e^{-2\eta^2}\right)u_1 - \frac{1}{\pi\sqrt{\pi}}\eta e^{-3\eta^2} - \frac{1}{2\pi\sqrt{\pi}}\eta e^{-3\eta^2} - \frac{3\sqrt{3}}{4\pi}\phi\left(\eta\sqrt{3}\right) + \\ & \left(1 - \frac{2}{\pi}\right)u_2 + \left(\frac{3\sqrt{3}}{4\pi} - \frac{1}{2}\right)u_1 \end{aligned} \tag{4.11}$$

Coefficients for Eq. (4.6–4.11) are given in Polubarinova-Kochina (1962) and repeated in Table 4.3.

Table 4.3. Coefficients for Series u_n for the Solution of the Boussinesq Analytical Equation (Polubarinova-Kochina 1962)

η	u_1	u_2	u_3
0	0.0000	0.0000	0.0000
0.1	0.1125	0.0141	-0.0039
0.2	0.2227	0.0160	-0.0081
0.3	0.3286	0.0073	-0.0090
0.4	0.4284	-0.0092	-0.0049
0.5	0.5205	-0.0300	0.0039
0.6	0.6039	-0.0519	0.0159
0.7	0.6778	-0.0718	0.0280
0.8	0.7421	-0.0874	0.0373
0.9	0.7969	-0.0975	0.0422
1.0	0.8427	-0.1017	0.0418
1.1	0.8802	-0.1004	0.0368
1.2	0.9103	-0.0946	0.0281
1.3	0.9340	-0.0855	0.0194
1.4	0.9523	-0.0744	0.0078
1.5	0.9661	-0.0626	-0.0011
1.6	0.9764	-0.0510	-0.0079
1.7	0.9838	-0.0394	-0.0125
1.8	0.9891	-0.0310	-0.0147
1.9	0.9928	-0.0232	-0.0151
2.0	0.9953	-0.0169	-0.0141
2.5	0.9996	-0.0024	-0.0047
3.0	0.9999	-0.0002	-0.0006
3.5	1.0000	0.0000	-0.0001
4.0	1.0000	0.0000	-0.0001

Two verification problems presented in this section also appear in the PORFLOW manual (ACRi 1994). The first simulates a recharge process by fixing the head 1 m above the initial phreatic surface; the second simulates a seepage process by fixing the head at the left boundary 1 m below the initial phreatic surface.

To obtain the analytical solution for the domain shown in Figure 4.5, values from Table 4.3 were substituted into Eq. (4.6–4.11). Similarly, in CFEST, the 1-D free-surface flow problem was set up as a rectangular domain. The horizontal extent (L_x) was set to 150 m, with a variable grid spacing that ranged from a minimum of 0.37 m at the left boundary to 5 m at the right boundary for a total of 44 nodes. The vertical extent (L_z) of the unconfined aquifer was set to 11 m across 16 grid nodes for the recharge problem and 10 m for the seepage problem. The minimum grid spacing was set to 0.1 m at the top boundary, which progressively increased to its maximum of 3 m at the bottom boundary. The grid refinement at the top boundary reduced the potential for numerical error near the phreatic surface.

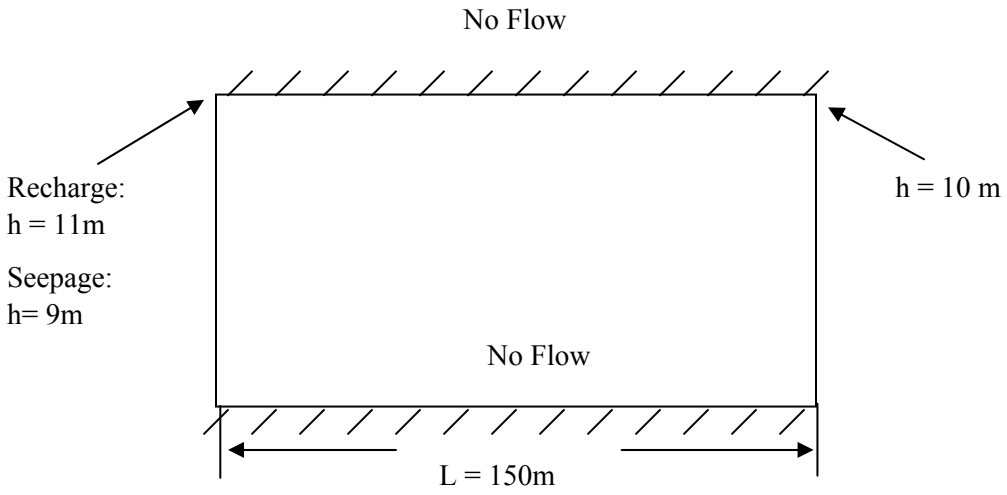

Figure 4.5. Diagrammatic Representation of the Free-Surface Problems

The phreatic surface was set to 10 m at all nodes except the left boundary, which was set as a Dirichlet boundary of 11 m for the recharge problem and 9 m for seepage. The right boundary of the phreatic surface was also set as a Dirichlet boundary. The top and bottom domain boundaries are no-flow boundaries, as shown with hash marks in Figure 4.5.

The total simulation time was 324 days with an initial time step of 0.01 day. The time step was then maintained at 0.02 day until the simulation reached one day, when it is increased to one-day increments.

The parameters used for the analytical and numerical solutions are summarized in Table 4.4. Because the analytical solution assumes horizontal flow, the vertical hydraulic conductivity is 100 times smaller than the horizontal hydraulic conductivity. The comparison between the analytical solution (solid lines) and CFEST solution (symbols) at 9, 36, 81, 144, 225, and 324 days is shown in Figure 4.6 for recharge and 4.7 for seepage. Agreement between analytical and numerical solutions for the data sets is excellent.

Table 4.4. Parameter Values Used in the Uniform Steady-State Flow Problem

Parameters	Units	Value
L_x	m	150
L_z	m	11 and 10[(a)]
Δx	m	$0.37 < \Delta x < 5$
Δz	m	$0.1 < \Delta z < 3.0$
K_x	m/day	0.1
K_z	m/day	1.0
θ	m^3/m^3	0.25
(a) The length of the vertical domain was 11 m for recharge and 10 m for seepage.		

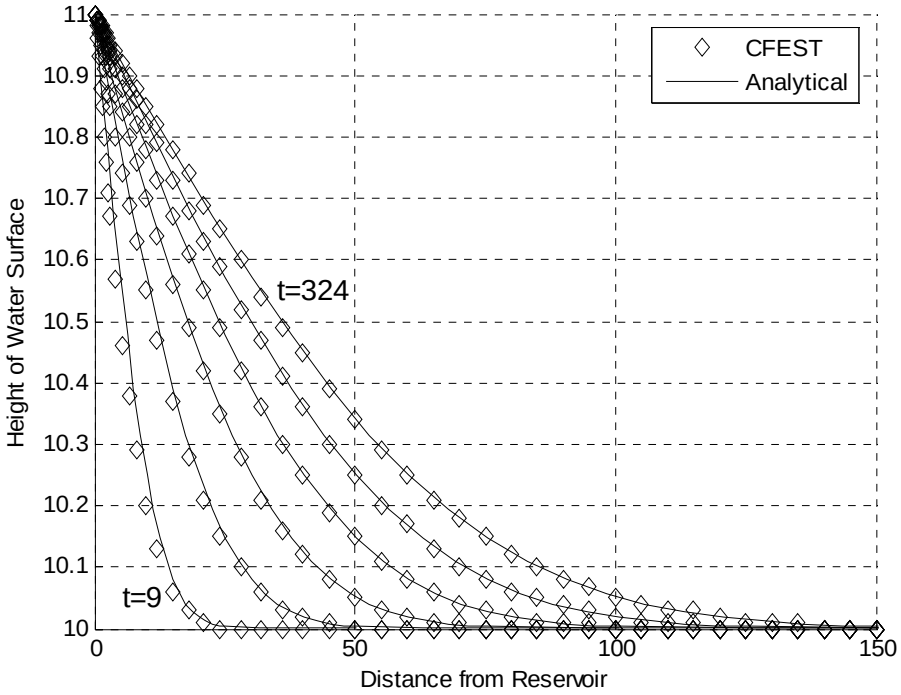

Figure 4.6. Time History of Phreatic Surface for Both Analytical and Numerical Solutions for the Recharge Problem

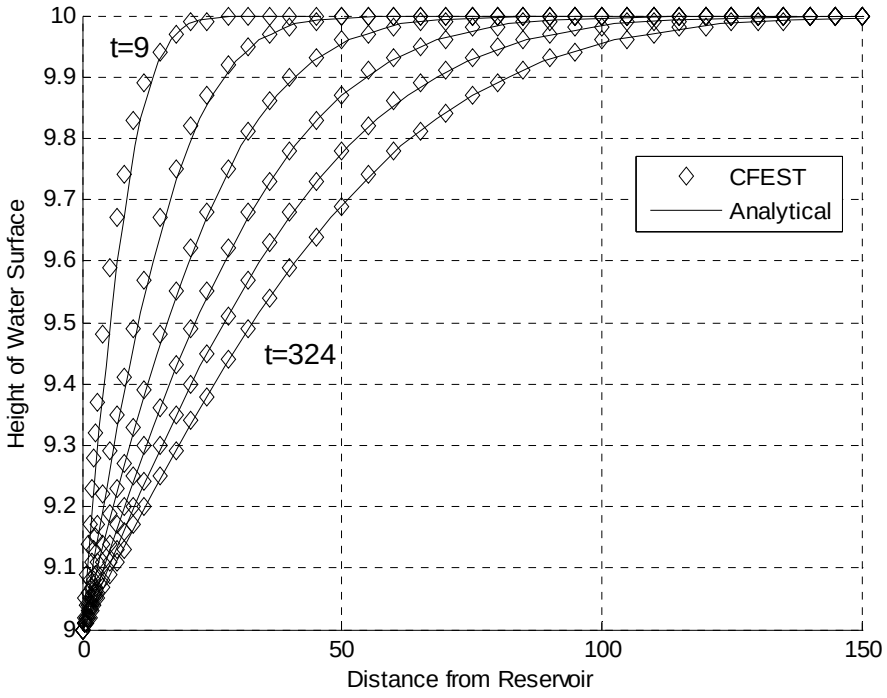

Figure 4.7. Time History of Phreatic Surface for Both Analytical and Numerical Solutions for the Seepage Problem

4.2 Solute Transport Verification

4.2.1 Dirichlet Upstream Boundary Condition, Linear Geometry

The classical transient, advection-dispersion problem can be expressed by the 1-D Ogata-Banks equation given as (Domenico and Schwartz 1990)

$$D_x \frac{\partial^2 C}{\partial x^2} - v\frac{\partial C}{\partial x} = \frac{\partial C}{\partial t} \tag{4.12}$$

where C is the concentration [M L^3], D is the dispersion coefficient [L^2 t^{-1}], and t and x represent time and distance, respectively. The linear pore water velocity, v [L t^{-1}], is further defined as

$$v = {q_x}/{\theta} \tag{4.13}$$

where q is the Darcy velocity [L t^{-1}], and θ is the porosity [L^3 L^{-3}]. The coefficient of dispersion is defined as

$$D_x = v\alpha_x \tag{4.14}$$

For the boundary conditions given as

$$C(0,t) = C_0 \tag{4.15a}$$

$$C(\infty,t) = 0 \tag{4.15b}$$

$$C(x,0) = 0 \tag{4.15c}$$

The 1-D analytical solution can be expressed as (Coats and Smith 1964)

$$\frac{C(x,t)}{C_o} = \frac{1}{2}\left[erfc\left(\frac{x - v_x t}{2\sqrt{D_x t}}\right) + \exp(\frac{x v_x}{D_x}) erfc(\frac{x + v_x t}{2\sqrt{D_x t}}) \right] \tag{4.16}$$

The first boundary condition in Eq. (4.15a) indicates that, at x = 0 for all time t, the concentration is C_o. This condition is represented by a Dirichlet, held-concentration boundary condition for a continuous source. The second boundary condition in Eq. (4.15b) indicates an infinitely large domain where the concentration far from the source is zero. The third boundary condition (Eq. 4.15c) is an initial condition that states that at all points x at time t = 0, the concentration is zero. That is, at the start of the simulation, C_o represents a sudden and uniformly applied solute source at the upstream boundary.

Results from the dimensionless, analytical solution given by Coats and Smith (1964) were compared with the results of the numerical CFEST simulations. The dimensionless solution of Eq. (4.16) is expressed as

$$\frac{C(x,t)}{C_0} = \frac{1}{2}\left[erfc\left(\frac{X - D\lambda}{2\sqrt{\lambda}} \right) + \exp(XD) \cdot erfc\left(\frac{X + D\lambda}{2\sqrt{\lambda}} \right) \right] \tag{4.17}$$

where X, D, and λ represent dimensionless quantities defined as

$$X = x / X_L \tag{4.18}$$

$$\lambda = t \frac{D_X}{\theta X_L{}^2} \tag{4.19}$$

$$D = \frac{v_x X_L}{D_x} \tag{4.20}$$

and X_L represents the maximum distance.

The simulation domain is shown in Figure 4.8. The domain length (L) is 60 m, with a uniform grid spacing of 5 m in the x direction. (i.e., 13 nodes in x direction). The total time of simulation is 800 days with a five-day time step. A Dirichlet boundary condition of 1 mol/kg is set for concentration at the left boundary, whereas the exit boundary concentration is held at zero. The hydraulic conductivity of the material is 10 m/day with a porosity of 0.1. The value of the dispersion coefficient is 16 m. The parameters used for analytical and numerical solutions are summarized in Table 4.5.

Figure 4.9 compares the analytical and CFEST numerical solutions. CFEST predictions for solute concentrations compare well throughout the simulation period but, in general, later times show better agreement with the analytical solution than early times.

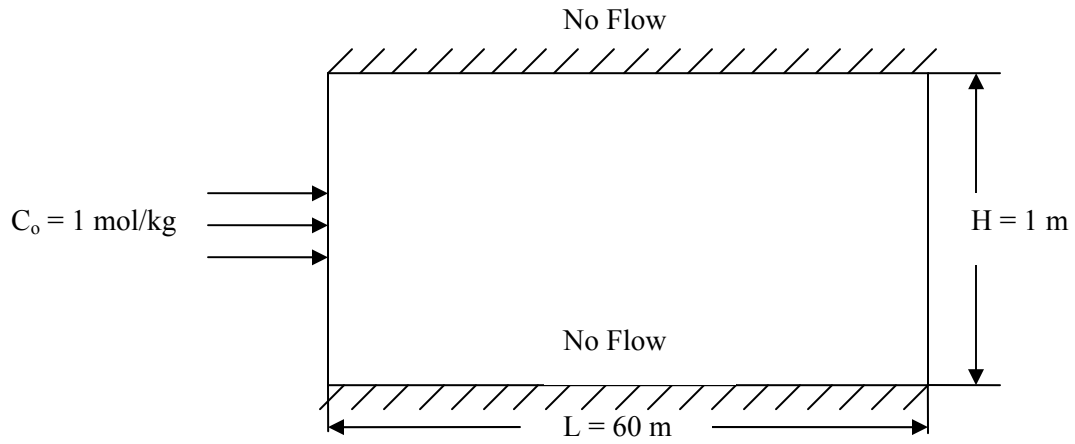

Figure 4.8. Problem Domain for Dirichlet Upstream Boundary Condition

Table 4.5. Parameter Values Used in the Dirichlet (held-concentration) Solute Transport Problem

Parameters	Units	Value
Δx	m	5
L	m	60
Δt	day	5
T	day	800
K	m/day	10
α_x	m	16
θ	m^3/ m^3	0.1
C_o	mol/kg	1.0

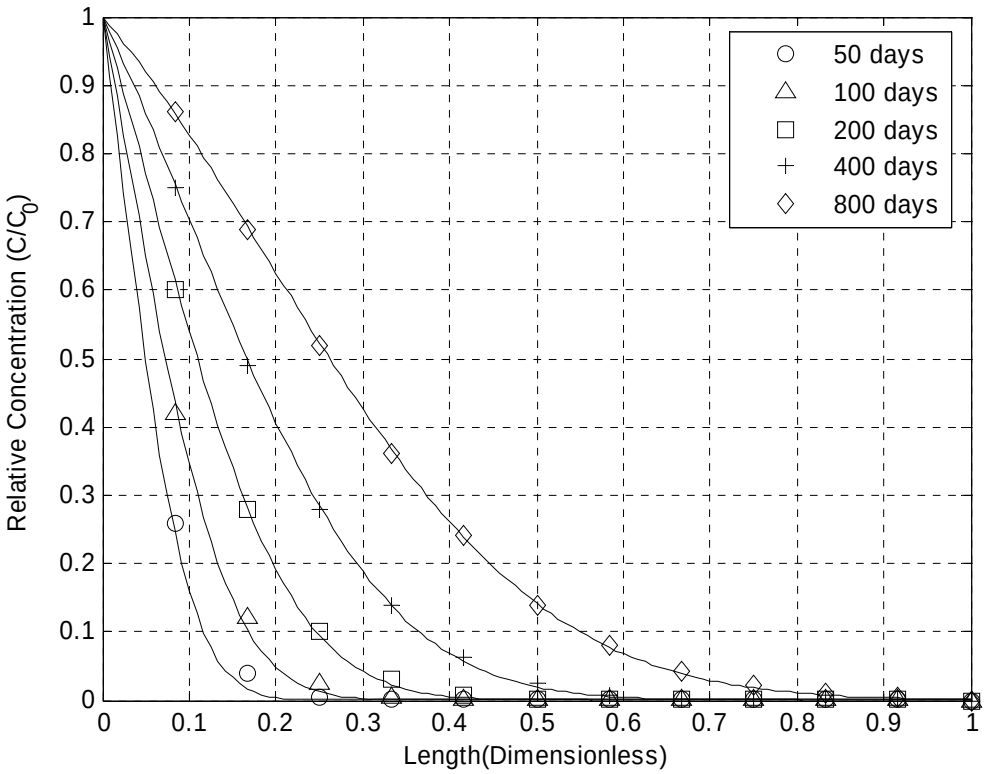

Figure 4.9. Comparison of Analytical (Coats and Smith 1964) and CFEST Solute Transport Solution with Dirichlet Boundary Conditions

4.2.2 Flux Concentration Boundary Condition for Solute Transport

Boundary and initial conditions for a mixed Dirichlet and flux condition at an upstream boundary for Eq. (4.12) are given as

$$C(0,t) = u_x \frac{\partial C}{\partial x} - D_x \frac{\partial C}{\partial x^2} \tag{4.21a}$$

$$C(\infty,t) = 0 \tag{4.21b}$$

$$C(x,0) = 0 \tag{4.21c}$$

The first boundary condition shown in Eq. (4.21a) states that at x = 0 for all time t the solute flux is specified by the quantity expressed on the right side of the equation. This is known as a Neumann boundary condition for a continuous source. The second boundary condition in Eq. (4.21b) indicates an infinitely large domain where the concentration far from the source is zero. This was represented in the numerical model as a Dirichlet boundary. The third boundary condition (Eq. 4.21c) is an initial condition that states that at all points x at time t = 0 the concentration is zero. That is, at the start of the simulation, C_o represents a sudden and uniformly applied solute flux at the upstream boundary. The solution for this boundary value problem is given by Coats and Smith (1964):

$$\begin{aligned}\frac{C(x,t)}{C_0} = \frac{1}{2}\left\{ erfc\left(\frac{x - v_x t}{2\sqrt{D_x t}}\right) - \exp\left(\frac{x v_x}{D_x}\right) erfc\left(\frac{x + v_x t}{2\sqrt{D_x t}}\right)\left[1 + \frac{v_x}{D_x}(x + v_x t)\right]\right\} \\ + v_x \sqrt{\frac{t}{D_x \pi}} \exp\left[-\frac{(x - v_x t)^2}{4 D_x t}\right]\end{aligned} \tag{4.22}$$

Results from the dimensionless analytical solution given by Coats and Smith (1964) were compared with the results of the numerical CFEST simulations. The dimensionless solution of Eq. (4.22) is expressed as

$$\begin{aligned}\frac{C(x,t)}{C_0} = \frac{1}{2}\left[erfc\left(\frac{\sqrt{\gamma}(X - \lambda)}{2\sqrt{\lambda}}\right) - \exp(\gamma X)\, erfc\left(\frac{\sqrt{\gamma}(X + \lambda)}{2\sqrt{\lambda}}\right)\left[1 + \gamma\left(X + \lambda\right)\right]\right] \\ + \sqrt{\frac{\gamma\lambda}{\pi}} \exp\left(-\frac{\left(X - \lambda\right)^2 \gamma}{4\lambda}\right)\end{aligned} \tag{4.23}$$

where the dimensionless parameter γ is defined as

$$\gamma = \frac{v_x X_L}{D_x} \tag{4.24}$$

and the dimensionless parameters X and λ were defined in Eq. (4.18) and (4.19), respectively.

The domain diagram is shown in Figure 4.10. A uniform grid spacing of 100 m in the x direction is used. The domain length *L* is 2000 m (i.e., 21 nodes in x direction) and is set at a large distance from the inlet so it does not affect simulation results in the upstream region. The total time of simulation is 800 days, with a uniform time step of 25 days. Solute mass, with a concentration of the injection fluid of 1 mol/kg, enters the domain a constant flux *Q* of 10 m^3/day. The head at the exit boundary (x = 2000) is fixed at zero. The parameters used for both the analytical and numerical solutions are summarized in Table 4.6.

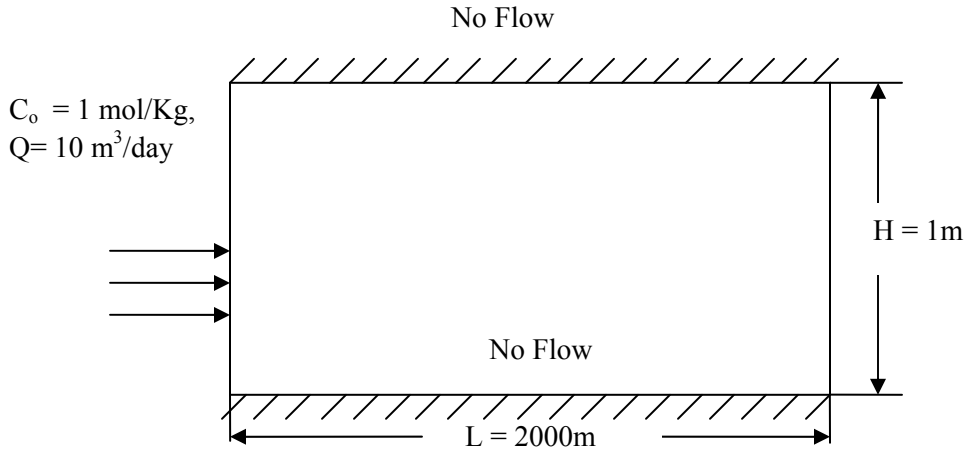

Figure 4.10. Problem Domain for Flux Concentration Boundary Condition

Table 4.6. Parameter Values Used in the Neumann (Flux) Solute Transport Problem

Parameters	Units	Value
Δx	m	100
L	m	2000
Δt	day	25
T	day	800
v	m^3/m^2/day	0.1
α_x	m	52
θ	m^3/m^3	0.1
C_o	mol/kg	1.0
Q	m^3/day	10

Figure 4.11 compares the analytical and CFEST numerical solutions. CFEST predictions for solute concentrations compare well throughout the simulation period but, in general, later times show better agreement with the analytical solution than early times.

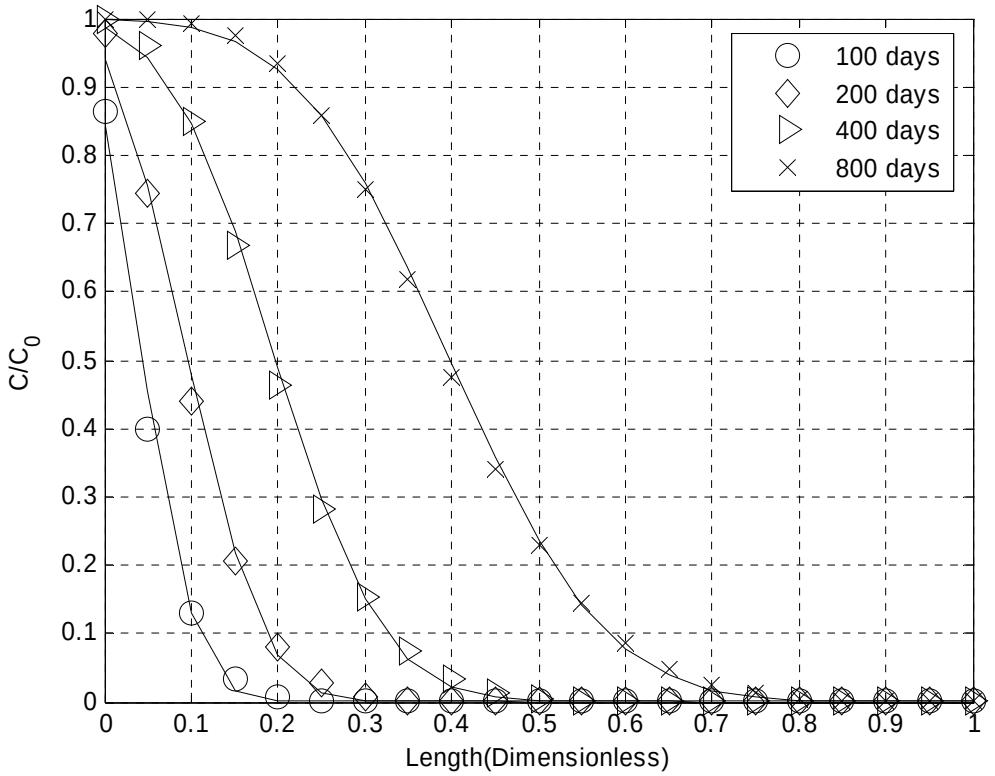

Figure 4.11. Comparison of Analytical (Coats and Smith 1964) and CFEST with a Flux Boundary Condition Imposed at the Inlet and a 25-Day Time Step Regime

4.3 Transient One-Dimensional Diffusion

In the absence of groundwater flow, solute transport may still occur due to molecular diffusion, a process that moves solutes from points of higher concentration toward points of lower concentration. An analytical dimensionless solution for 1-D diffusion is given by Carslaw and Jaeger (1959):

$$\frac{C}{C_o} = 1 - \frac{4}{\pi}\sum_{n=0}^{\infty}\frac{(-1)^n}{2n+1}e^{-(2n+1)^2\pi^2 T/4}\cos\frac{(2n+1)\pi\zeta}{2} \qquad 4.25$$

where T and ζ are dimensionless parameters of time and distance, respectively. The concentration ratio (C/C_o) in Eq. (4.25) for time T at 0.02, 0.05, 0.1, 0.2, 0.5, and 1.0 was compared with the CFEST numerical solution for equivalent times.

For the numerical solution, a rectangular homogeneous domain was used to simulate solute diffusive transport. The schematic for this problem is shown in Figure 4.12. The top, bottom, and left edges were set up as no-flow boundaries, so contaminants could not cross these boundaries. The concentration was set to zero everywhere in the domain and unity at the right boundary. A uniform grid spacing of 0.05 m in the x direction was used (i.e., 21 nodes), and the total time of simulation was 1. The time step was 0.0005 from 0 to 0.1, and 0.005 thereafter (see Table 4.6).

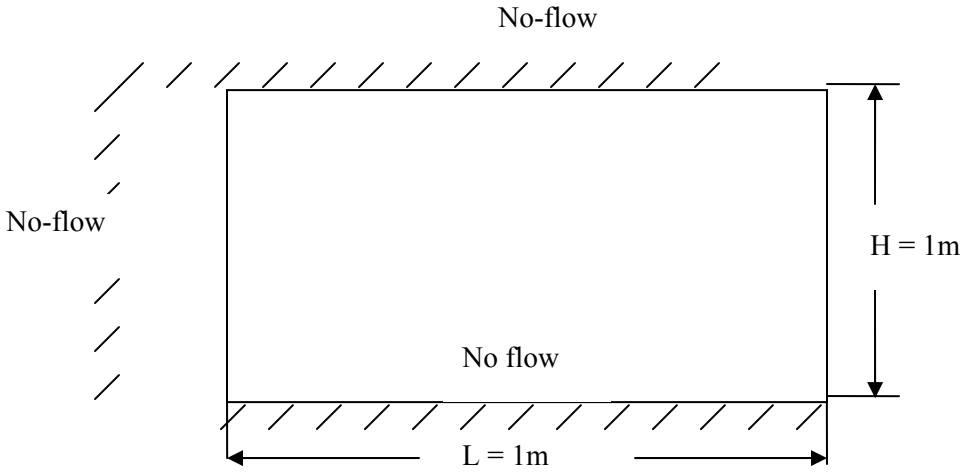

Figure 4.12. Problem Domain for Solute Diffusive Transport

For ease of comparison with the dimensionless analytic solution, both the porosity and the molecular diffusivity were set to unity. Dispersivities were set to zero, and the retardation coefficient (*R*) to one. These values are summarized with other parameter values in Table 4.7. Solute effects on fluid density were also ignored.

Table 4.7. Parameter Values Used in the Diffusive Transport Problem

Parameters	Units	Value
t	day	1
Δt	day	0.0005 and 0.005
Δx	m	0.05
L	m	1
α_x	m	0
R	dimensionless	1
θ	m^3/m^3	1
D_d	m^2/t	1

Figure 4.13 shows the relative concentration curves for distinct time planes for both the analytical (solid lines) and the CFEST simulations (symbols). The numerical results demonstrate excellent agreement with the analytical solution.

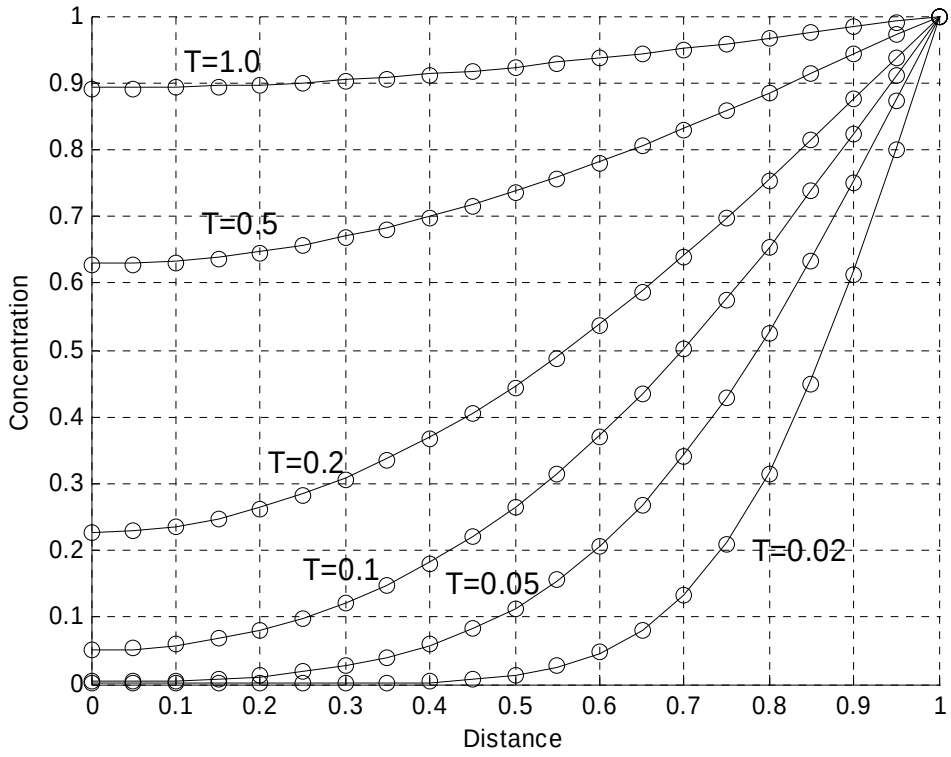

Figure 4.13. Concentration Profile at Selected Dimensionless Times (T) = 0.02, 0.05, 0.1, 0.2, 0.5, and 1

4.3.1 Uranium-234 Decay

Chemical constituents in groundwater may undergo decay due to radioactive disintegration. The process of decay can be described as a first-order kinetic rate law where the rate of decay of the mass is expressed as a function of its current mass. When related to a unit volume of the phase, the rate of decay is related to the current concentration. The residence time of mass in groundwater is described mathematically as

$$t = -\frac{\ln\left(\frac{C}{C_o}\right)}{\lambda} \tag{4.26}$$

where the first-order radioactive decay constant for both the free and sorbed solute, λ [t^{-1}], is defined as

$$\lambda = \frac{\ln(2)}{t_{1/2}} \tag{4.27}$$

where $t_{1/2}$ is the solute half-life, the time for the chemical to decay to half its original concentration.

To verify the accuracy of CFEST in simulating decay in a porous medium, the numerical solution in CFEST was compared with an exact analytical solution of CMM (Hydrogeologic 1991) as cited in the

FRAC3DVS theory guide (Thierren 2001). Because only one solute can be transported in the current version of CFEST, the three-member chain decay problem presented by Thierren was modified here to focus only on the transport of uranium-234.

The problem domain is shown in Figure 4.14. A 1-D domain was set up with a total length (L) of 500 m and a unit depth in y and z. A uniform grid spacing of 5 m in the x direction is used for a total of 101 nodes. The total simulation time was 10,000 years, with a uniform time step of 20 years. The retardation factor of U^{234} is 1.43×10^4, and the half-life is 2.47×10^5 years. The initial concentration (C_0) of uranium-234 is 1 mol/kg. The parameters used in the CFEST numerical solution are summarized in Table 4.8. Figure 4.15 shows the concentration profile for uranium-234 at a time of 10,000 years for both CFEST and the capability maturity model solutions. It can be seen that the results of the analytical and numerical solutions are in agreement.

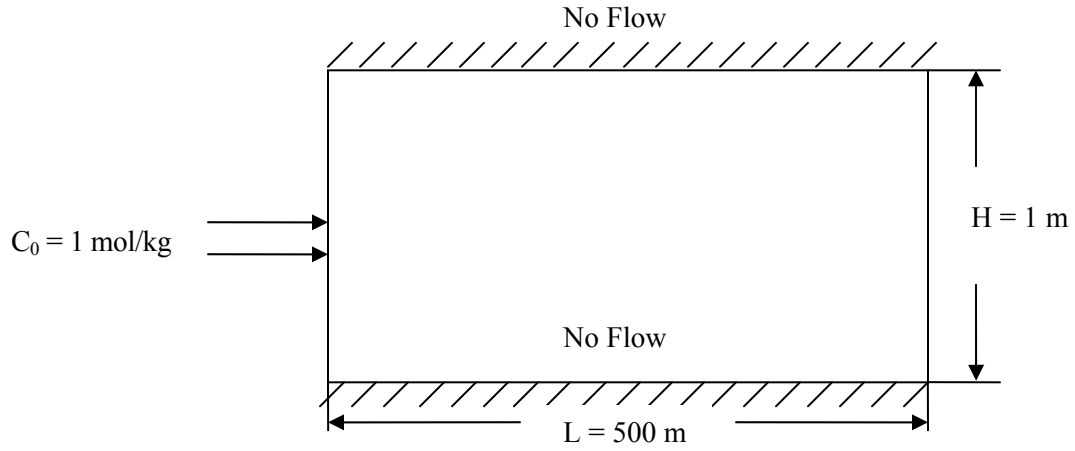

Figure 4.14. Problem Domain for Uranium-234 Decay Problem

Table 4.8. Parameter Values Used in the Uranium-234 Decay Problem

Parameters	Units	Value
t	yr	10,000
Δt	m	5
Δx	m	500
L		
C_o	mol/kg	1.0
α_x	m	10
R	dimensionless	1.43×10^4
$t_{½}$	yr	2.47×10^5
θ	m^3/m^3	0.1
D_d	m^2/t	0

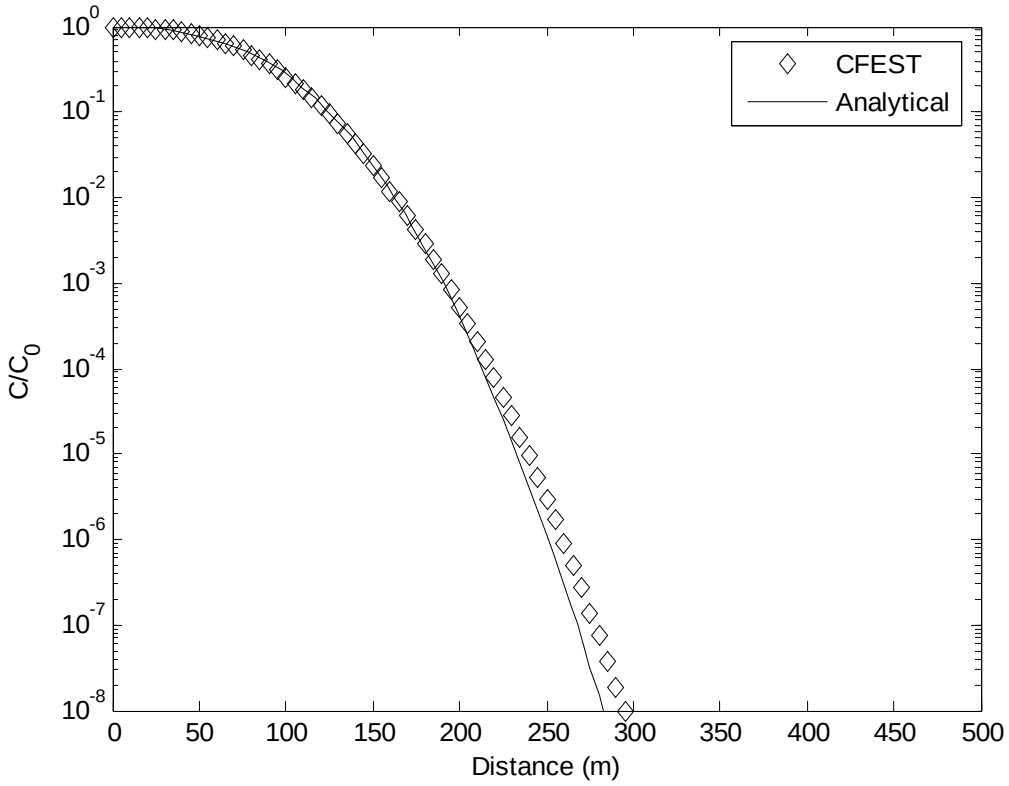

Figure 4.15. Relative Concentration Profile for Uranium-234 at 10,000 Years for Both the Analytical Solution and CFEST Numerical Solution

4.3.2 Density-Dependent Flow and Solute Transport (Seawater Intrusion)

Henry's problem (Henry 1964a, b) describes the advance of a diffused saltwater wedge in a confined aquifer initially filled with fresh water. Fresh water enters at a constant rate from the inland boundary, mixes with intruding seawater, and discharges to the sea through the vertical coast boundary. Seawater intrudes form the coastal boundary, advances, and mixes with the discharging fresh water.

The simulation domain is shown in Figure 4.16. The dimensionless analytical solution of Segol (1994) is used for comparing the numerical results generated by CFEST for Henry's problem. The rectangular domain length (L) is 2 m, the height (H) 1 m, with a uniform grid spacing of 0.1 m (i.e., 21 nodes in x direction and 11 nodes in z direction). No-flow boundaries are set at the top and bottom boundaries to represent a confined aquifer. Initially, the domain contains only fresh water. A source of fresh water is injected at the left inland boundary at a rate of $Q_{in} = 6.6 \times 10^{-5}$ m^2/s and a concentration of $C_{in} = 0$. At the coastal boundary, a Dirichlet boundary is set with a hydrostatic seawater pressure equivalent to the density of seawater ($\rho_{sea} = 024.99$ kg/m^3). Seawater entering the vertical coastal boundary has a concentration of $C_{sea} = 0.0357$ mol/kg.

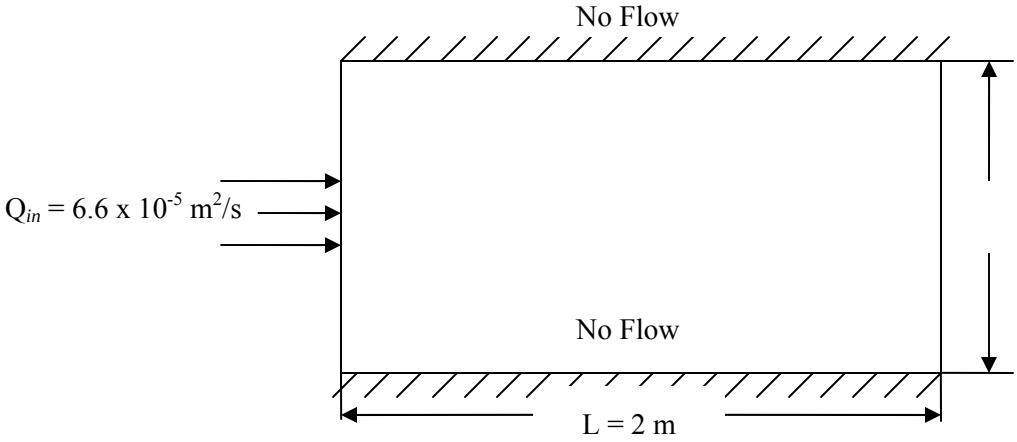

Figure 4.16. Henry's Problem Domain

Two different values of molecular diffusivity are used for comparing the numerical and analytical solutions, $D_m = 18.8571 \times 10^{-6}$ m^2/s and $D_m = 6.6 \times 10^{-6}$ m^2/s, where the total Henry's dispersion coefficient (D) is defined as the product of molecular diffusivity and porosity ($D = \varepsilon D_m$).

The total simulation time is 100,000 seconds to ensure steady-state conditions had been reached, with a uniform time step of 500 seconds. The parameters used for simulation are summarized in Table 4.9.

Table 4.9. Parameter Values Used in Henry's Problem

Parameters	Units	Value
Δx	m	0.1
L	m	2
Δz	m	0.1
H	m	1
Δt	second	500
T	second	100,000
K	m/s	0.01
D_m	m^2/s	6.6×10^{-6} 18.87×10^{-6}
k	m^2	1.0204×10^{-9}
$\alpha_L=\alpha_T$	m	0
θ	m^3/m^3	0.35
Q_{in}	kg/s	6.6×10^{-2}
ρ_0	kg/m^3	1000
ρ_{sea}	kg/m^3	1024.99
C_o	mol/kg	0
Csea	mol/kg	0.0357

Isochlors for the seawater intrusion problem are shown in Figure 4.17 for both values of the diffusion coefficient. Figure 4.17 shows that the CFEST numerical solution with symbols and Segol's analytical solution (solid lines) are in very close agreement. The symbols representing the concentration contours for the numerical solution are not evenly spaced along the contour line because the data points were extracted from contour lines generated by the Tecplot[(a)] plotting program.

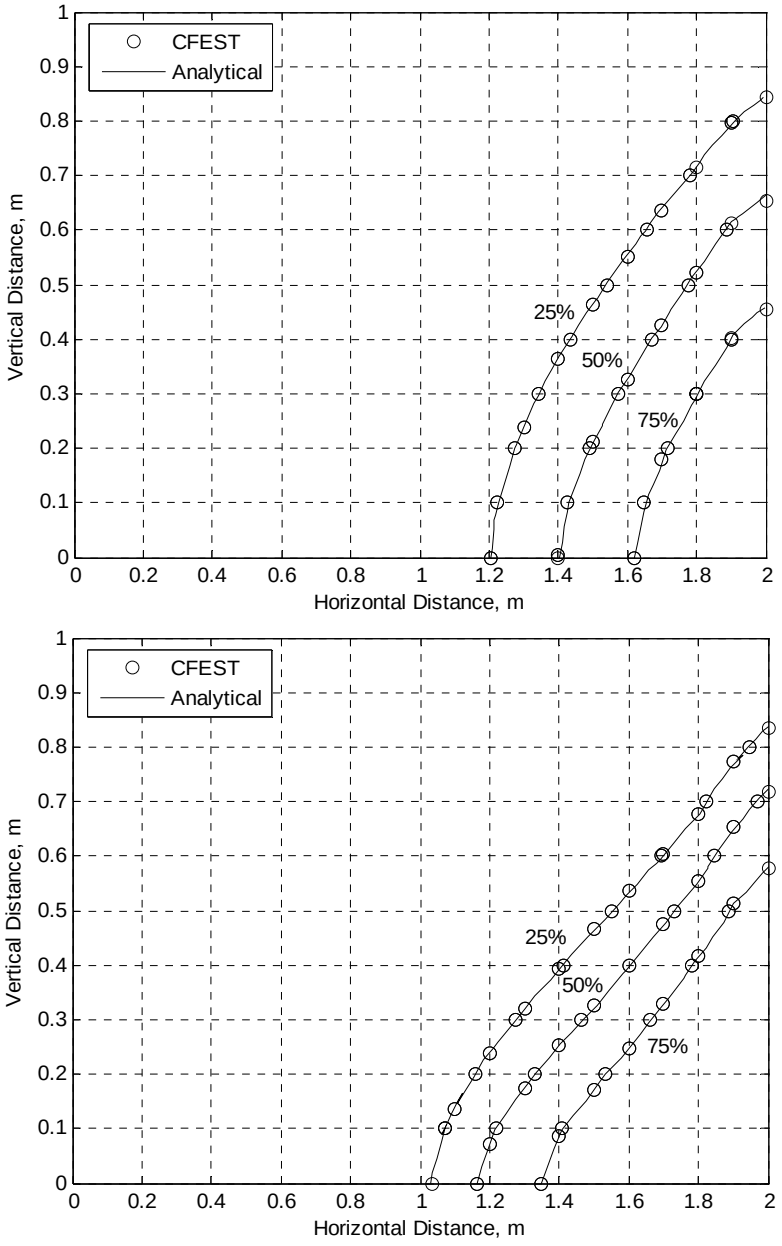

Figure 4.17. Isochlors for CFEST and Segol's Analytical Solution for Henry's Problem Using Diffusion Coefficients of a) 18.8571×10^{-6} m^2/s and b) 6.6×10^{-6} m^2/s.

(a) Tecplot, Inc. 2004. Tecplot, Version 10.0. Tecplot, Bellevue, Washington.

5.0 Literature Cited

Analytic & Computational Research, Inc. (ACRi). 1994. *PORFLOW Validation Version 2.50*. ACRi, Bel Air, California.

Balay S, K Buschelman, V Eijkhout, WD Gropp, D Kaushik, MG Knepley, LC McInnes, BF Smith, and H Zhang. 2004. *PETSc Users Manual.* ANL-95/11 Rev. 2.1.5, Argonne National Laboratory, Argonne, Illinois.

Bear J. 1979. *Hydraulics of Groundwater*. McGraw-Hill, New York.

Carslaw HS and JC Jaeger. 1959. *Conduction of Heat in Solids* (2nd ed.). Oxford University Press, London.

Coats KH and DB Smith. 1964. "Dead-End Pore Volume and Dispersion in Porous Media." *Society of Petroleum Engineering Journal,* 4(1):73-84.

Domenico PA and FW Schwartz. 1990. *Physical and Chemical Hydrogeology*. John Wiley & Sons, New York.

Freeze RA and JA Cherry. 1979. *Groundwater.* Prentice-Hall, Englewood Cliffs, New Jersey.

Gupta SK, CR Cole, CT Kincaid, and AM Monti. 1987. *Coupled Fluid, Energy, and Solute Transport (CFEST) Model: Formulation and User's Manual.* BMI/ONWI-660, Battelle Memorial Institute, Columbus, Ohio.

Gupta SK. 1997. *Draft User's Manual, CFEST-96 Flow and Solute Transport, Constant/Variable Density, Computationally Efficient, and Low Disk PC/Unix Version*. Consultant for Environmental System Technologies, Irvine, California.

Henry HR. 1964a. "Interfaces Between Salt Water and Fresh Water in Coastal Aquifers." *Sea Water in Coastal Aquifers.* Water-Supply Paper 1613-C, U.S. Geological Survey, Washington, D.C. pp. C35-C70.

Henry HR. 1964b. "Effects of Dispersion on Salt Encroachment in Coastal Aquifers." *Sea Water in Coastal Aquifers*. Water-Supply Paper 1613-C, U.S. Geological Survey, pp. C71-C84.

Huyakorn PS and GF Pinder. 1983. *Computational Methods in Subsurface Flow*. Academic Press, San Diego, California.

INTERCOMP Resource Development and Engineering, Inc. 1976. *A Model for Calculating Effects of Liquid Waste Disposal in Deep Saline Aquifers.* Publication No. 26903, National Technical Information Service, Washington, D.C.

Pinder GF and WG Gray. 1977. *Finite Element Simulation in Surface and Subsurface Hydrology*. Academic Press, New York.

Polubarinova-Kochina PY. 1962. *Theory of Groundwater Movement*. Translated from Russian by R.J.M. DeWiest. Princeton University Press, Princeton, New Jersey.

Ross B, JW Mercer, SD Thomas, and BH Lester. 1982. *Benchmark Problems for Repository Siting Models.* NUREG/CR-3097, U.S. Nuclear Regulatory Commission, Washington, D.C.

Scheidegger AE. 1961. "General Theory of Dispersion in Porous Media." *Journal of Geophysical Research,* 66(10):3273–3278.

Segol G. 1994. *Classic Groundwater Simulations: Proving and Improving Numerical Models*. Prentice-Hall, Englewood Cliffs, New Jersey.

Theis CV. 1935. "The Relation Between the Lowering of the Piezometric Surface and the Rate and Duration of Discharge of a Well Using Groundwater Storage." *Transactions of the American Geophysical Union,* 2:519-524.

Therrien R, EA Sudicky, and RG McLaren. 2001. *FRAC3DVS: An Efficient Simulator for Three-Dimensional, Saturated-Unsaturated Groundwater Flow and Density-Dependent, Chain-Decay Solute Transport in Porous, Discretely-Fractured Porous or Dual-Porosity Formations. Mathematical Theory and Verification.* Universite Laval, Quebec, Canada.

Tsang CF, T Buscheck, and C Doughty. 1980. *Aquifer Thermal Energy Storages: A Numerical Simulation of Auburn Field Experiments.* LBL-10210, Lawrence Berkeley Laboratory, Berkeley, California.

Young D and D Kincaid. 1981. "The ITPACK Package for Large Sparse Linear Systems. *Elliptic Problem Solvers,* M Schultz (Ed.). Academic Press, New York, pp. 163–185.

Voss CI and WR Souza. 1987. "Variable Density Flow and Solute Transport Simulation of Regional Aquifers Containing a Narrow Freshwater-Saltwater Transition Zone." *Water Resources Research*, 23(10):1851–1866.

Zienkiewicz OC and RL Taylor. 2000. *The Finite Element Method Volume 1–The Basis* (5th ed.). Butterworth-Heinemann, Oxford, United Kingdom.

Distribution

No. of Copies		
3	DOE-Richland Operations Office	
	D.R. Hildebrand	A6-38
	J.G. Morse	A6-38
	M. Thompson	A6-38
2	CH2M HILL Hanford Group, Inc.	
	F.J. Anderson	E6-35
	F.M. Mann	E6-35
3	Fluor Hanford Co.	
	J.V. Borghese	E6-35
	M.E. Byrnes	E6-35
	B.J. Ford	E6-35
2	DOE Office of River Protection	
	R.W. Lober	H6-60
	S.A. Wiegman	H6-60

No. of Copies		
20	Pacific Northwest National Laboratory	
	R.W. Bryce	K9-35
	Y. Chen	K9-36
	C.R. Cole	K9-36
	V.L. Freedman (4)	K9-36
	E.J. Freeman	K9-36
	M.D. Freshley	K9-33
	C.T. Kincaid	K9-33
	C.J. Murray	K6-81
	W.E. Nichols	K9-36
	P.D. Thorne	K9-33
	V.R. Vermeul	K6-96
	D.L. Ward	K9-36
	M.D. Williams	K6-96
	S.K. Wurstner	K9-36
	Z.F. Zhang	K9-36
	Information Release (2)	P8-55